Journal of Maps

ISSN: (Print) (Online) Journal homepage: www.tandfonline.com/journals/tjom20

The high-resolution map of Oxia Planum, Mars; the landing site of the ExoMars Rosalind Franklin rover mission

Peter Fawdon, Csilla Orgel, Solmaz Adeli, Matt Balme, Fred J. Calef, Joel M. Davis, Alessandro Frigeri, Peter Grindrod, Ernst Hauber, Laetitia Le Deit, Damien Loizeau, Andrea Nass, Cathy Quantin-Nataf, Elliot Sefton-Nash, Nick Thomas, Ines Torres, Jorge L. Vago, Matthieu Volat, Sander De Witte, Francesca Altieri, Andrea Apuzzo, Julene Aramendia, Gorka Arana, Rickbir Singh Bahia, Steven G. Banham, Robert Barnes, Alexander M. Barrett, Wolf-Stefan Benedix, Anshuman Bhardwaj, Sarah Jane Boazman, Tomaso R. R. Bontognali, John Bridges, Benjamin Bultel, Valérie Ciarletti, Maria Cristina De Sanctis, Zach Dickeson, Elena A. Favaro, Marco Ferrari, Frédéric Foucher, Walter Goetz, Albert F. C. Haldemann, Elise Harrington, Angeliki Kapatza, Detlef Koschny, Agata M. Krzesinska, Alice Le Gall, Stephen R. Lewis, Tanya Lim, Juan Manuel Madariaga, Benjamin James Man, Lucia Mandon, Nicolas Mangold, Javier Martin-Torres, Joseph D. McNeil, Antonio Molina, Andoni G. Moral, Sara Motaghian, Sergei Nikiforov, Nicolas Oudart, Andrea Pacifici, Adam Parkes Bowen, Dirk Plettemeier, Pantelis Poulakis, Alfiah Rizky Diana Putri, Ottaviano Ruesch, Lydia Sam, Christian Schröder, Christoph Statz, Rebecca Thomas, Daniela Tirsch, Zsuzsanna Toth, Stuart Turner, Martin Voelker, Stephanie C. Werner, Frances Westall, Barry J. Whiteside, Adam Williams, Rebecca M. E. Williams, Jack Wright & Maria-Paz Zorzano

To cite this article: Peter Fawdon, Csilla Orgel, Solmaz Adeli, Matt Balme, Fred J. Calef, Joel M. Davis, Alessandro Frigeri, Peter Grindrod, Ernst Hauber, Laetitia Le Deit, Damien Loizeau, Andrea Nass, Cathy Quantin-Nataf, Elliot Sefton-Nash, Nick Thomas, Ines Torres, Jorge L. Vago, Matthieu Volat, Sander De Witte, Francesca Altieri, Andrea Apuzzo, Julene Aramendia, Gorka Arana, Rickbir Singh Bahia, Steven G. Banham, Robert Barnes, Alexander M. Barrett, Wolf-Stefan Benedix, Anshuman Bhardwaj, Sarah Jane Boazman, Tomaso R. R. Bontognali, John Bridges, Benjamin Bultel, Valérie Ciarletti, Maria Cristina De Sanctis, Zach Dickeson, Elena A. Favaro, Marco Ferrari, Frédéric Foucher, Walter Goetz, Albert F. C. Haldemann, Elise Harrington, Angeliki Kapatza, Detlef Koschny, Agata M. Krzesinska, Alice Le Gall, Stephen R. Lewis, Tanya Lim, Juan Manuel Madariaga, Benjamin James Man, Lucia Mandon, Nicolas Mangold, Javier Martin-Torres, Joseph D. McNeil, Antonio Molina, Andoni G. Moral, Sara Motaghian, Sergei Nikiforov, Nicolas Oudart, Andrea Pacifici, Adam Parkes Bowen, Dirk Plettemeier, Pantelis Poulakis, Alfiah Rizky Diana Putri, Ottaviano Ruesch, Lydia Sam, Christian Schröder, Christoph Statz, Rebecca Thomas, Daniela Tirsch, Zsuzsanna Toth, Stuart Turner, Martin Voelker, Stephanie C. Werner, Frances Westall, Barry J. Whiteside, Adam Williams, Rebecca M. E. Williams, Jack Wright & Maria-Paz Zorzano (2024) The high-resolution map of Oxia Planum, Mars; the landing site of the ExoMars Rosalind Franklin rover mission, Journal of Maps, 20:1, 2302361, DOI: 10.1080/17445647.2024.2302361

To link to this article: https://doi.org/10.1080/17445647.2024.2302361

JOURNAL OF MAPS
2024, VOL. 20, NO. 1, 2302361
https://doi.org/10.1080/17445647.2024.2302361

Taylor & Francis
Taylor & Francis Group

SCIENCE

OPEN ACCESS Check for updates

The high-resolution map of Oxia Planum, Mars; the landing site of the ExoMars Rosalind Franklin rover mission

Peter Fawdon [a], Csilla Orgel [b], Solmaz Adeli [c], Matt Balme [d], Fred J. Calef [e], Joel M. Davis [f], Alessandro Frigeri [g], Peter Grindrod [h], Ernst Hauber [i], Laetitia Le Deit [j], Damien Loizeau [k], Andrea Nass [l], Cathy Quantin-Nataf [m], Elliot Sefton-Nash [n], Nick Thomas [o], Ines Torres [m,p], Jorge L. Vago [q], Matthieu Volat [m], Sander De Witte[r], Francesca Altieri [s], Andrea Apuzzo [s,t], Julene Aramendia [u], Gorka Arana [v], Rickbir Singh Bahia [w], Steven G. Banham [x], Robert Barnes [y], Alexander M. Barrett [z], Wolf-Stefan Benedix [aa], Anshuman Bhardwaj [ab], Sarah Jane Boazman [ac], Tomaso R. R. Bontognali [ad,ae], John Bridges [af], Benjamin Bultel [ag], Valérie Ciarletti [ah], Maria Cristina De Sanctis [ai], Zach Dickeson [aj,ak], Elena A. Favaro [al], Marco Ferrari [am], Frédéric Foucher [an], Walter Goetz [ao,ap], Albert F. C. Haldemann [aq], Elise Harrington [ar,as], Angeliki Kapatza [at], Detlef Koschny [au,av], Agata M. Krzesinska [aw], Alice Le Gall [ax,ay], Stephen R. Lewis [az], Tanya Lim [ba], Juan Manuel Madariaga [bb], Benjamin James Man [bc], Lucia Mandon [bd,be], Nicolas Mangold [bf], Javier Martin-Torres [bg,bh], Joseph D. McNeil [bi], Antonio Molina [bj], Andoni G. Moral [bk], Sara Motaghian [f,bl], Sergei Nikiforov [bm], Nicolas Oudart[bn], Andrea Pacifici [bo], Adam Parkes Bowen [bp], Dirk Plettemeier [bq], Pantelis Poulakis[br], Alfiah Rizky Diana Putri [bs,bt], Ottaviano Ruesch [bu], Lydia Sam [bv], Christian Schröder [bw], Christoph Statz [bx], Rebecca Thomas [by], Daniela Tirsch [bz], Zsuzsanna Toth [ca], Stuart Turner [cb,cc], Martin Voelker[cd], Stephanie C. Werner [ce], Frances Westall [cf], Barry J. Whiteside [cg], Adam Williams[ch], Rebecca M. E. Williams [ci], Jack Wright [cj] and Maria-Paz Zorzano [ck]

[a]School of Physical Sciences, Open University, Milton Keynes, UK; [b]European Space Research and Technology Centre (ESA/ESTEC), Directorate of Human and Robotic Exploration, Noordwijk, The Netherlands; [c]Institute of Planetary Science, German Aerospace Center (DLR), Berlin, Germany; [d]School of Physical Sciences, Open University, Milton Keynes, UK; [e]Jet Propulsion Laboratory, California Institute of Technology, Pasadena, CA, USA; [f]Department of Earth Sciences, Imperial College London, London, UK; [g]Istituto di Astrofisica e Planetologia Spaziali, Istituto Nazionale di Astrofisica, Rome, Italy; [h]Department of Earth Sciences, Natural History Museum, London, UK; [i]German Aerospace Center (DLR), Institute of Planetary Research, Berlin, Germany; [j]Nantes Université, Univ Angers, Le Mans Université, CNRS, Laboratoire de Planétologie et Géosciences, Nantes, France; [k]Université Paris Saclay – CNRS – Institute d'Astrophysique Spatiale, Orsay, France; [l]German Aerospace Center (DLR), Institute of Planetary Research, Berlin, Germany; [m]Laboratoire de Géologie de Lyon, Université Claude Bernard Lyon 1, CNRS, ENS Lyon; [n]European Space Research and Technology Centre (ESA/ESTEC), Directorate of Science, Noordwijk, The Netherlands; [o]Physikalisches Institut, University of Bern, Bern, Switzerland; [p]European Space Agency (ESA/ESTEC), Noordwijk, The Netherlands; [q]European Space Agency (ESA/ESTEC), Noordwijk, The Netherlands; [r]European Space Agency (ESA/ESTEC), Noordwijk, The Netherlands; [s]Istituto di Astrofisica e Planetologia Spaziali, Istituto Nazionale di Astrofisica, Rome, Italy; [t]Università degli Studi di Roma Tre, Roma, Italy; [u]Department of Analytical Chemistry, University of the Basque Country (UPV/EHU), Leioa, Spain; [v]Department of Analytical Chemistry, University of the Basque Country (UPV/EHU), Leioa, Spain; [w]European Space Agency (ESA/ESTEC), Noordwijk, The Netherlands; [x]Department of Earth Sciences, Imperial College London, London, UK; [y]Department of Earth Sciences, Imperial College London, London, UK; [z]School of Physical Sciences, Open University, Milton Keynes, UK; [aa]Technische Universität Dresden, Dresden, Germany; [ab]School of Geosciences, University of Aberdeen (UK), Aberdeen, UK; [ac]European Space Agency (ESA/ESTEC), Noordwijk, The Netherlands; [ad]Space Exploration Institute, Neuchâtel, Switzerland; [ae]Department of Environmental Sciences, University of Basel, Basel, Switzerland; [af]Space Research Centre, School of Physics and Astronomy, University of Leicester, Leicester, UK; [ag]Centre for Earth Evolution and Dynamics (CEED), Department of Geosciences, University of Oslo, Oslo, Norway; [ah]LATMOS/IPSL, UVSQ Université Paris-Saclay, Sorbonne Université, CNRS, Paris, France.; [ai]Istituto di Astrofisica e Planetologia Spaziali, Istituto Nazionale di Astrofisica, Rome, Italy; [aj]Department of Earth Sciences, Natural History Museum, London, UK; [ak]Department of Earth and Planetary Sciences, Birkbeck College, University of London, London, UK; [al]School of Physical Sciences, Open University, Milton Keynes, UK; [am]Istituto di Astrofisica e Planetologia Spaziali, Istituto Nazionale di Astrofisica, Rome, Italy; [an]CNRS, Centre de Biophysique Moléculaire, Orléans, France; [ao]Planetary Science Department, Max Planck Institute for Solar System Research (MPS), Goettingen, Germany; [ap]Max Planck Institute for Solar System Research (MPS), Goettingen, Germany; [aq]European Space Research and Technology Centre (ESA/ESTEC), Directorate of Human and Robotic Exploration, Noordwijk, The Netherlands; [ar]Centre for Earth Evolution and Dynamics (CEED), Department of Geosciences, University of Oslo, Oslo, Norway; [as]National Oceanography Centre, University of Southampton, Southampton, UK; [at]Department of Physics and Astronomy, University College London, London, UK; [au]European Space Agency (ESA/ESTEC), Noordwijk, The Netherlands; [av]TUM School of Engineering and Design, TU Munich, Garching, Germany; [aw]Centre for Earth Evolution and Dynamics, Department of Geosciences, University of Oslo, Oslo, Norway; [ax]LATMOS/IPSL, UVSQ Université Paris-Saclay, Sorbonne Université, CNRS, Paris, France; [ay]Institut Universitaire de France, Paris, France; [az]School of Physical Sciences, Open University, Milton Keynes, UK; [ba]European Space Agency (ESA), European Space Astronomy Centre (ESAC), Madrid, Spain; [bb]Department of Analytical Chemistry, University of the Basque Country (UPV/EHU), Leioa, Spain; [bc]School of Physical Sciences, Open University, Milton Keynes, UK; [bd]LESIA, Observatoire de Paris, Université PSL, CNRS, Sorbonne Université, Université de Paris, Meudon, France; [be]Division of Geological and Planetary Sciences, California Institute of Technology, Pasadena, CA, USA; [bf]Laboratoire de Planétologie et Géodynamique, CNRS, Nantes, France; [bg]Department of Planetary Sciences, School of Geosciences, University of Aberdeen, King's College, Aberdeen, UK; [bh]Instituto Andaluz de Ciencias de la Tierra (CSIC-UGR), Granada, Spain; [bi]School of Physical Sciences, Open University, Milton Keynes, UK; [bj]Centro de Astrobiología (CAB) CSIC/INTA, Madrid, Spain; [bk]INTA. Instituto Nacional de Técnica Aeroespacial, Madrid, Spain; [bl]Department of Earth

Sciences, Natural History Museum, London, UK; [bm]Space Research Institute of the Russian Academy of Sciences (IKI), Moscow, Russia; [bn]LATMOS/IPSL, UVSQ Université Paris-Saclay, Sorbonne Université, CNRS, Paris, France; [bo]International Research School of Planetary Sciences, Università Gabriele D'Annunzio, Pescara, Italy; [bp]Space Research Centre, University of Leicester, Leicester, UK; [bq]Technische Universität Dresden, Dresden, Germany; [br]European Space Agency (ESA/ESTEC), Noordwijk, The Netherlands; [bs]Planetary and Atmospheric Sciences, Sumatra Institute of Technology, South Lampung, Indonesia; [bt]Imaging Group, Mullard Space Science Laboratory, University College London, Surrey, UK; [bu]Institut für Planetologie, Westfälische Wilhelms Universität Münster, Münster, Germany; [bv]School of geosciences (UK), University of Aberdeen, Aberdeen, UK; [bw]Biological and Environmental Sciences, University of Stirling, Stirling, UK; [bx]Technische Universität Dresden, Dresden, Germany; [by]Institute of Psychiatry, Psychology & Neuroscience, King's College London, London, UK; [bz]Institute of Planetary Research, German Aerospace Center (DLR), Berlin, Germany; [ca]Deep BV, Amsterdam, Netherlands; [cb]AstrobiologyOU, School of Environment, Earth and Ecosystem Sciences, The Open University, Milton Keynes, UK; [cc]The James Hutton Institute, Aberdeen, UK; [cd]European Space Astronomy Center, Madrid, Spain; [ce]Centre for Earth Evolution and Dynamics (CEED), Department of Geosciences, University of Oslo, Oslo, Norway; [cf]CNRS-Centre de Biophysique Moléculaire, Orléans, France; [cg]UCL Mullard Space Science Laboratory, Dorking, UK; [ch]ESA European Space Opperations Center, Darmstadt, Germany; [ci]Planetary Science Institute, Tucson, AZ, USA; [cj]European Space Agency (ESA), European Space Astronomy Centre (ESAC), Madrid, Spain; [ck]Centro de Astrobiología (CSIC-INTA), Madrid, Spain

ABSTRACT

This 1:30,000 scale geological map describes Oxia Planum, Mars, the landing site for the ExoMars *Rosalind Franklin* rover mission. The map represents our current understanding of bedrock units and their relationships prior to *Rosalind Franklin's* exploration of this location. The map details 15 bedrock units organised into 6 groups and 7 textural and surficial units. The bedrock units were identified using visible and near-infrared remote sensing datasets. The objectives of this map are (i) to identify where the most astrobiologically relevant rocks are likely to be found, (ii) to show where hypotheses about their geological context (within Oxia Planum and in the wider geological history of Mars) can be tested, (iii) to inform both the long-term (hundreds of metres to ~1 km) and the short-term (tens of metres) activity planning for rover exploration, and (iv) to allow the samples analysed by the rover to be interpreted within their regional geological context.

ARTICLE HISTORY
Received 24 October 2023
Revised 21 December 2023
Accepted 1 January 2024

KEYWORDS
ExoMars; Oxia Planum; Mars; Geological Map; Astrobiology; Rosalind Franklin Rover

1. Introduction

1.1. Introduction

Oxia Planum is the landing site for the European Space Agency's (ESA) ExoMars rover mission (Vago et al., 2018). The missions goal is to search for signs of past and present life. To accomplish this, the ExoMars rover, called *Rosalind Franklin*, will investigate the geochemical environment in the shallow subsurface – the rover is equipped with a drill to retrieve samples from as deep as 2 m – using its 'Pasteur' suite of scientific instruments during Rosalind Franklins nominal surface mission of 218 sols (Vago et al., 2017).

In anticipation for the surface mission, the ExoMars Rover Science Operations Working Group (RSOWG) established a 'Macro' sub-group dedicated to preparations for operations relating to orbital and rover remote sensing data analyses. The rover can drive 30–100 m per day, depending on the terrain's complexity, so it is important to (1) characterise the landing site with metre-scale fidelity – relevant for day to day rover operations, – and (2) to cover an area encompassing the uncertainty ellipse for likely landing locations (which has an area in the order of ~1000 km^2). The search for signs of life by the rover is predicated on identifying the best possible sites for assessing three parameters: (1) geological context consistent with life-hospitable conditions, (2) potential physical biosignatures, and (3) potential chemical biosignatures.

To achieve this, the RSOWG Macro group organised a two-phase, high-resolution geologic mapping group campaign (Sefton-Nash et al., 2020) focused on the 'one-sigma' landing ellipse (*i.e.* an ~66.75 × 5 km ellipse with ~67% touchdown probability) with in Oxia Planum. The campaign consisted of an initial 'group mapping' phase, where team members mapped one or more 1 km square 'quads', followed by a 'reconciliation phase'. In the group mapping phase, the principal objectives were (i) to familiarise scientists with the geography and geology of the landing site, and (ii) to collect observations to create a geological map to build and guide the mission's strategic planning. The end goal is making the best use of the available mission resources (*e.g.* time, energy, locomotion range, data) to identify locations for sample acquisition and analysis. In the reconciliation phase, the phase 1 observations were reassessed to create a consistent map description of the geology. The reconciliation phase incorporated interpretations from elsewhere in the 3-sigma landing ellipse (*i.e.* the ~ 100 × 20 km ellipse with 99% touchdown probability) and beyond.

The wider goals of this project are (i) to develop a thorough understanding of the landing site's geography and geological history prior to operations, (ii) to formulate site-specific testable hypotheses to facilitate interpretation of mission results, and (iii) to map locations where those hypotheses could be tested. This map will therefore be vital for both

CONTACT Peter Fawdon peter.fawdon@open.ac.uk School of Physical Sciences, Open University, Milton Keynes, Buckinghamshire MK7 6AA, UK
Supplemental map for this article is available online at https://doi.org/10.1080/17445647.2024.2302361

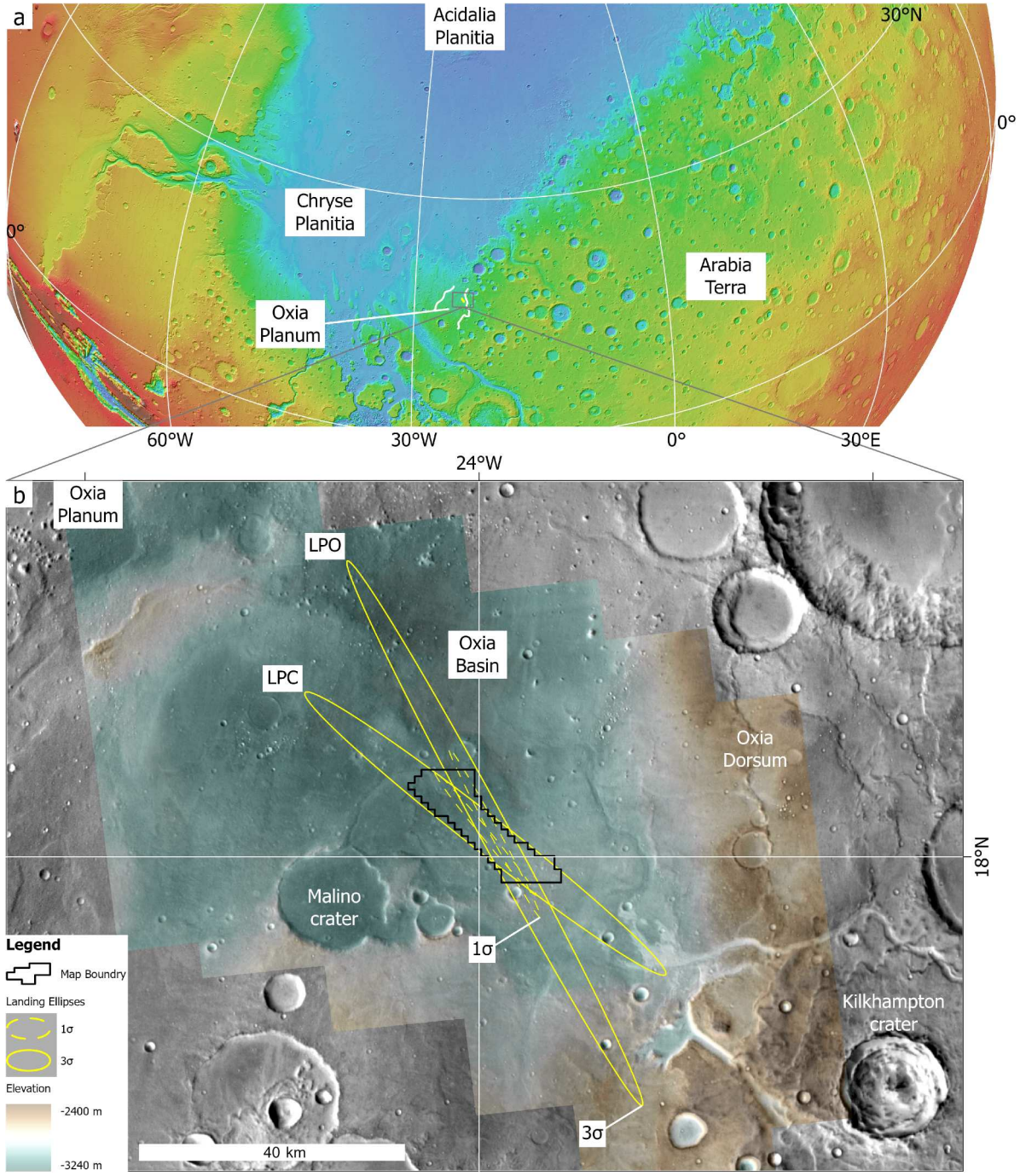

Figure 1. Location. The location of the high-resolution map of the landing site in Oxia Planum, Mars (A) Topographic map showing Oxia Planum on the northern margin of Arabia Terra. White lines mark NW-SE extent. (B) Topographic map (CTX DTM from Fawdon et al., 2021) overlain on THEMIS mosaic showing the extent of the mapping area within Oxia Planum. The 1 and 3 sigma landing ellipses are show in yellow. The different ellipse azimuths represent the start (high azimuth – LPO) and close (low azimuth – LPC) of the planned launch window, with many more ellipses (not shown) aligned between these extremes reflecting launch at any time within the launch window.

contextualising the scientific analysis of the rover samples. Here we present the completed map including descriptions and the stratigraphic relationship of map units and discuss how its intended use for rover operations, planning and future scientific study.

1.2. Context

Oxia Planum is situated on the northern margin of Arabia Terra (Fawdon et al., 2021; Figure 1) and preserves a record of the diverse geological processes that have shaped the region. It is a transitional region between the heavily cratered Noachian-aged Arabia Terra (>3.7 Ga); (Hartmann & Neukum, 2001; Tanaka et al., 2014) and the younger low-lying Hesperian/Amazonian-aged plains of Chryse Planitia (<3.0 Ga). The landing site was selected because of its abundance of Noachian-aged material, including regional phyllosilicate-bearing deposits (Carter et al., 2015, 2023; Favaro et al., 2024; Noe Dobrea et al., 2010; Riu

et al., 2023), which provide evidence for widespread aqueous alteration (Brossier et al., 2022; Mandon et al., 2021; Quantin-Nataf et al., 2021), and occurs at a sufficiently low elevation to permit landing (Vago et al., 2018). Oxia Planum's geology records Noachian basement (Pan et al., 2019; Quantin-Nataf et al., 2021) and global-scale tectonic fabrics (Anderson et al., 2001; Woodley et al., 2023). The wider region was extensively modified during the late Noachian and Hesperian periods, as shown by evidence of fluvial and paleo-lake activity (Davis et al., 2023; Fawdon et al., 2022; Gary-Bicas & Rogers, 2021; Mandon et al., 2021; Molina et al., 2017; Quantin-Nataf et al., 2021), possible shoreline formation (e.g. Dickeson & Davis, 2020), volcanism (Michalski & Bleacher, 2013), and aqueous alteration (Bultel et al., 2019; Carter et al., 2015). Since then, the surface has been and continues to be shaped by aeolian transport and erosion processes (E. A. Favaro et al., 2021; Silvestro et al., 2021) and by impact cratering (Roberts et al., 2021; Uthus, 2020). The previous mapping efforts (Ivanov et al., 2020; Mastropietro, 2019; Quantin-Nataf et al., 2021; Tanaka et al., 2014; Uthus, 2020; detailed in Section 4.2) have not considered Oxia Planum at a scale relevant to rover operations. However, this map, and future companion publications, will directly link characterisation of the landing site at the highest possible resolution to hypothesis about the processes that formed it, derived from remote sensing data of the region.

2. Materials and methods

2.1. Location and projection

The main map covers an area from 17.11°N to 19.15°N and from 334.60°E to 336.60°E (Figure 1). The map is presented at 1:30,000, with digital products are available as vector and raster layers with a vertex spacing of 4 m and pixel size of 1 m in an equirectangular projection centred at 18.20°N, 335.45°E, based on the IAU Mars2000 sphere (available through Fawdon et al., 2021). This matches the coordinate system used by the ExoMars Rover Operations Control Centre (ROCC) to minimise local distortion. This is important for maintaining accuracy between remote sensing observation and rover scale operations.

2.1.1. High resolution imaging science experiment (HiRISE)

The map was created from a base-map mosaic (Volat & Quantan-Nataf, 2020; Figure 2) of red-channel HiRISE (McEwen et al., 2007) orthoimages and digital elevation models (DEMs) created using HiRISE stereo pairs following the method of Kirk et al. (2008) detailed in Fawdon et al. (2021) and Volat and Quantan-Nataf (2020). The HiRISE mosaic was georeferenced to a 6 m/pixel Context Camera (CTX; Malin, 2007) DEM and orthoimage mosaic (Fawdon et al., 2021) which in turn has been georeferenced to the 12 m/pixel High-Resolution Stereo Camera (HRSC; Gwinner et al., 2016; Neukum & Jaumann, 2004) MC11W regional mosaic (DLR, 2019) and MOLA spheroid (Neumann et al., 2003; Smith et al., 2001). The HiRISE mosaic was used to control Phase 1 mapping line work and all other data used were georeferenced to it. This ensures metre-scale spatial consistency between the various datasets. Where available, individual HiRISE Stereo DEMs, ortho images, Infrared, Red, Blue (IRB) and synthetic colour (RGB) data were used on top of the Volat et al. (2022) mosaic to provide additional information. These data used in Phase 2 reconciliation were georeferenced to the orthorectified red-channel image mosaic and are listed in Table 1 and any further information will be made available on request to the corresponding author.

2.1.2. Colour and stereo surface imaging system (CaSSIS)

The CaSSIS (Thomas et al., 2017) camera has four filters (IR; 950 nm, NIR; 850 nm, PAN; 650 nm and BLUE–GREEN; 475 nm), which provide a multispectral capability sensitive to a variety of minerals (Tornabene et al., 2017). We used all available CaSSIS data (Table 2) for the Phase 2 Oxia Planum work, but found the Near, Pan, Blue (NPB) band combination to be particularly useful. NPB images were georeferenced as described in Fawdon et al. (2021).

2.2. Making the map

The two-phase approach that we applied is similar to that used in geological assessment of the Mars 2020 landing site (Stack et al., 2020). The mapping focused on the one-sigma landing ellipse and covered the range of ellipse azimuths (the arrival azimuth rotates depending on the launch date within the approximately two-week-long launch window). This relatively small area was chosen in an effort to balance the human resources required to map at a level of fidelity relevant to the scale of rover operations (characterising variation in geology over tens of metres) and the infeasibility of the whole 3-sigma pattern of landing ellipses. In the event that the rover lands outside our mapped region, a rapid reconnaissance mapping (RRM; Balme et al., 2019) protocol is being developed in which a dedicated team will quickly map the terrain in a small region around the landing location. RRM will use the geological framework already established in this work to extend our understanding to the new location. This approach is possible because the 'one sigma' ellipse region is geologically representative of the wider area within Oxia Planum (Fawdon et al., 2021).

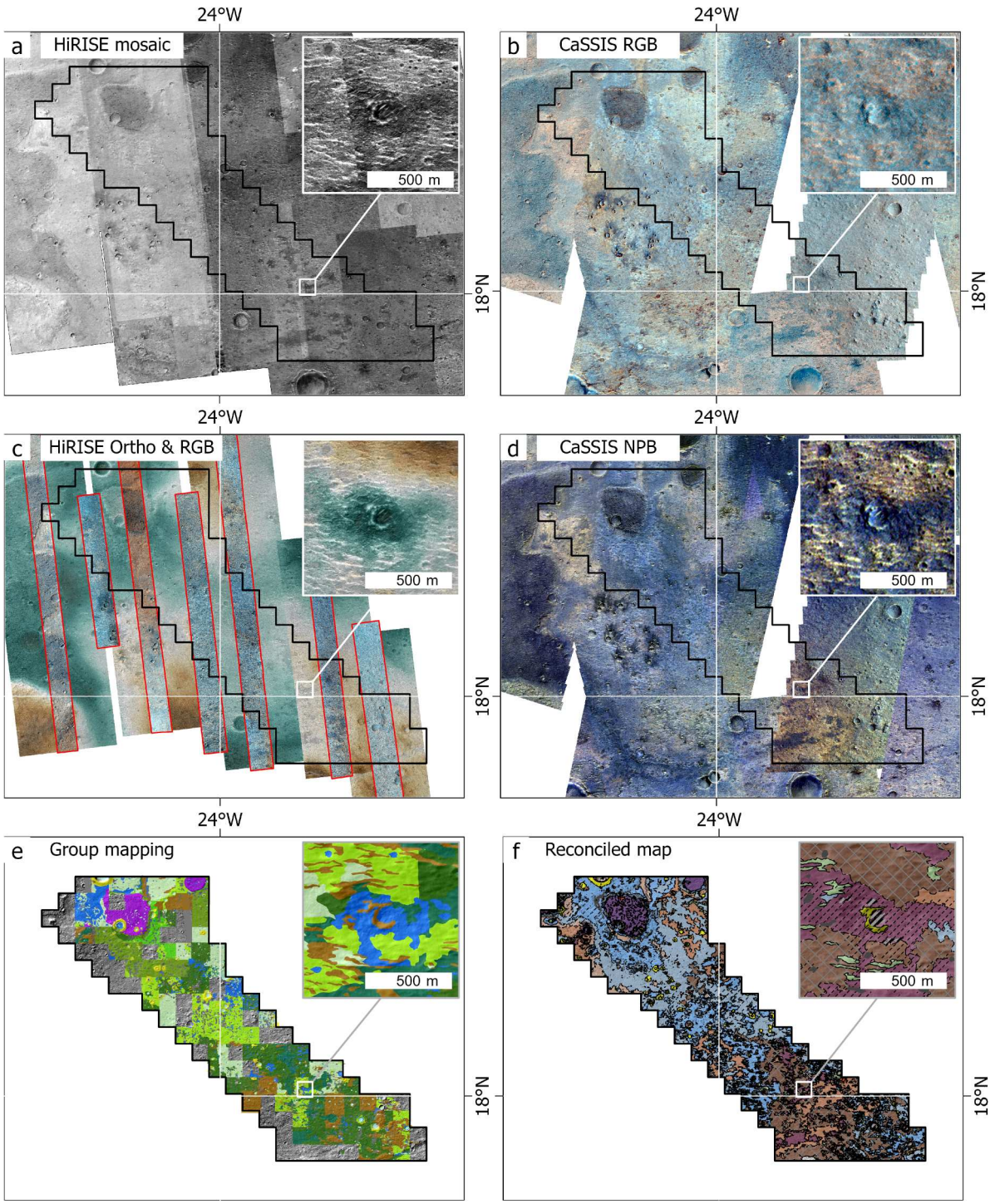

Figure 2. Basemap and data. Data used in Phase 1 (group) and Phase 2 (reconciliation) of the mapping. Insets show the 1 × 1 km^2 group mapping quad size. (a) HiRISE red-channel orthoimage mosaic (the DEM covers the same area; Volat & Quantan-Nataf, 2020) and (b) CaSSIS RGB mosaic (Fawdon et al., 2021) used for Phase 1. (c) HiRISE red-channel orthoimages and DEMs (Table 1), HiRISE colour images (Table 2) and (d) CaSSIS NPB mosaic (Table 3) used in Phase 2. (e) Completed Quads from the Phase 1 group mapping prior to reconciliation and (f) showing the Phase 2 final reconciliation output.

2.2.1. Group mapping

In Phase 1 group mapping, 75 volunteers (noted as 'Mapping team' in the author list) associated with the RSOWG (first 19 authors in the author list) followed a programme of four training sessions on mapping practice and contextual geology, four area discovery meetings on designated mapping areas, and a pre-mapping meeting in June 2020. Then, before mapping started, mappers were presented with a 'unit guide' based on preliminary observations of the main units and features. The exercise organisers also provided the mappers with the mapping symbology and conventions to be used. The quad grid and naming conventions for the geography of Oxia Planum were also established in this phase and reported in Fawdon et al. (2021).

Table 1. HiRISE DEMs images.

Stereo images (*Ortho images)	Centre (Lat, Long)	Emission angle (°)	Pixel size (m)	EVP (m)	Data
PSP_009735_1985*	18.20°N 335.48°E	8.4°	0.285		www.uahirise.org/PSP_009735_1985
PSP_009880_1985	18.20°N 335.48°E	7.8°	0.285		www.uahirise.org/PSP_009880_1985
	18.20°N 335.40°E		1.000		www.uahirise.org/dtm/PSP_009880_1985
ESP_037558_1985*	18.21°N 335.57°E	15.4°	0.293		www.uahirise.org/ESP_037558_1985
ESP_036925_1985	18.24°N 335.57°E	1.1°	0.283		www.uahirise.org/ESP_036925_1985
	18.20°N 335.50°E		1.000		www.uahirise.org/dtm/ESP_036925_1985
ESP_039299_1985*	18.22°N 335.67°E	7.5°	0.284		www.uahirise.org/ESP_039299_1985
ESP_047501_1985	18.23°N 335.67°E	21.3°	0.302		www.uahirise.org/ESP_047501_1985
	18.22°N 335.60°E		1.000		www.uahirise.org/dtm/ESP_039299_1985
ESP_048648_1985*	18.14°N 335.76°E	9.0°	0.287		www.uahirise.org/ESP_048648_1985
ESP_040433_1985	18.13°N 335.76°E	18.3°	0.297		www.uahirise.org/ESP_040433_1985
ESP_064195_1985*	18.047° 335.813°	30.7°	0.325		www.uahirise.org/ESP_064195_1985
ESP_064195_1985	18.01°N 335.82°E	0.5°	0.283		www.uahirise.org/ESP_047435_1985

Note: HiRISE stereo DEM and ortho images used in addition to the basemap of Volat et al. (2022) to support digitisation during the reconciliation phase shown in Figurer 2(c).

Table 2. CaSSIS data used observations.

Image ID	Filters	Incidence angle (°)	Local time	Solar longitude (L_s)
MY34_003806_019_2	PAN-NIR-BLU	53.027	09:52:13	260.06
MY35_006504_018_0	PAN-NIR-BLU	74.907	06:51:39	22.62
MY35_008275_165_0	PAN-NIR-BLU	16.007	10:56:45	87.07
MY35_008742_019_0	PAN-RED-NIR-BLU	47.860	15:24:50	104.06
MY35_009481_165_0	PAN-NIR-BLU	24.363	13:42:46	132.27
MY35_013584_163_0	PAN-NIR-BLU	32.105	11:33:20	328.27

Note: CaSSIS observations used for mapping during the reconciliation phase shown in Figure 2(d).

The 75 volunteers were then assigned quads to map at a fixed scale of 1:2000. Mapping was completed in the NASA/JPL authored open-source Multi-Mission Geographic Information System (MMGIS; Calef et al., 2017; Calef & Soliman, 2019) with additional functionality for geospatial analysis and mapping, 'CAmpaign Mapping and Planning' (CAMP) developed for the NASA Mars 2020 rover mission. The ESA ExoMars team uploaded the required data and configurations necessary to facilitate group mapping to MMGIS/CAMP. The base-map datasets used for this Phase were the HiRISE orthoimage and DEM mosaics (Volat & Quantan-Nataf, 2020) and the CaSSIS colour mosaic (Fawdon et al., 2021). Between June 2020 and August 2020, the mapping volunteers concurrently mapped geologic contacts and surface features in 2D and with a supplementary 3D projection of the data to each complete one or more quads and wrote a 'quad abstract' recording their observations (Figure 2).

2.2.2. Reconciliation

In this phase, a small team (the two lead authors, in conjunction with advice from the lead authors) reconciled the scientific observations and linework made by the individual mappers to create a unified set of interpretations and a final map product. Reconciliation consisted of two steps.

In the first step, data ingestion, the geological units, contact and feature linework, and points of interest

Table 3. HiRISE RGB images.

Stereo images (*Ortho images)	Centre (Lat, Long)	Georeferenced Data	Data
ESP_057681_1985	18.22°N 335.53°E	https://maps.arcgis.com/home/item.html?id=f38969f34f40441b86f03eaee05de609	www.uahirise.org/ESP_057681_1985
PSP_009735_1985	18.20°N 335.48°E	https://maps.arcgis.com/home/item.html?id=6390accf8e5148e7aa434a699ca1bb83	www.uahirise.org/PSP_009735_1985
ESP_048648_1985	18.14°N 335.76°E	https://maps.arcgis.com/home/item.html?id=bbb9b66fccb14ef1886367c938d0f9e8	www.uahirise.org/ESP_048648_1985
ESP_064195_1985	18.05°N 335.81°E	https://maps.arcgis.com/home/item.html?id=728a864080094055847d68fca9fb9a67	www.uahirise.org/ESP_064195_1985
ESP_062402_1985	18.17°N 335.63°E	https://maps.arcgis.com/home/item.html?id=598ecdd8036f4b43814b7d1e42263145	www.uahirise.org/ESP_062402_1985
ESP_047501_1985	18.23°N 335.67°E	https://maps.arcgis.com/home/item.html?id=760c81dc6f8849db80d5b05b0784ada4	www.uahirise.org/ESP_047501_1985
ESP_036925_1985	18.20°N 335.57°E	https://maps.arcgis.com/home/item.html?id=1f393b8fda8242428a9a817d000c818d	www.uahirise.org/ESP_036925_1985

Note: HiRISE RGB images used to support digitisation during the reconciliation phase shown in Figure 2(c). Available though are online web map https://arcg.is/0y4bSa.

recorded by the volunteer mappers were ingested into ArcGIS Pro (v. 2.9–3.1) GIS software along with new HiRISE DEM and orthoimages (Table 1), new CaSSIS colour data (Table 3), CRISM and OMEGA hyperspectral data summary products (see: Brossier et al., 2022; Carter et al., 2015, 2023; Mandon et al., 2021; Parkes-Bowen et al., 2022; Quantin-Nataf et al., 2021) describing the distribution of hydrated minerals to support reconciliation. In addition, certain classes from the machine-learning terrain classification maps of the NOAH-H (Novelty Or Anomaly Hunter-HiRISE) project (Barrett et al., 2022, 2023) were used, mainly those representing aeolian bedforms and boulder fields.

In the second, scientific decision-making step, the insights from the volunteer mappers, recorded in their 'Quad abstracts' were fused with new observations and new contacts digitised at a fidelity appropriate for rover operations. To achieve this input from the mappers was as a 'field slip' line work redrawn to a consistent scale and style by the lead authors to create the reconciled 'fair copy' map (e.g.; Barnes & Lisle, 2013). The map digitisation was conducted in Arc Pro in 2D alongside concurrent 3D local scenes to guid the placement of unit boundaries. Mapping following US Geological Survey planetary mapping conventions (e.g. Skinner et al., 2022) adapted to meet the aims of the study at a scale of 1:2000. The geology of Oxia Planum is highly variable over short (tens of metres) scales but homogenous over long (kilometre or greater) scales. Units were challenging to discriminate and map at a large enough scale to be relevant to rover operations because of the textural and tonal heterogeneity over short, 10's m, length scale compared to the homogeneity over length scales of 1 km to 10 of km. In addition to the bedrock groups, summary overlays of surficial features and units were created based upon the NOAH-H results, constrained by new human observations. These mapping decisions are discussed in Section 4.1.

2.2.3. Visualisation choices

The selection of colours and symbology decisions were made to enable the ease of communication across the diverse international science team. Bedrock groups where coloured to intuitively follow their appearance in CaSSIS data with group that covered small areas of the map (E.g.; DM, BM and MM) given high contrast hues to aid identification whilst respecting reader sensitivity (such as colour blindness). Impact related material is yellow to follow the global conventions with red added as the sequential end member denoting the most recent events. Within each group the strongest hue denotes the recent unit as per (Skinner et al., 2022). Three line styles denote our confidence in the existence and location of each unit boundary. These range from 'inferred' – where logically a boundary should be located, through 'uncertain' – where we can tell a boundary is present, but it is not directly observed to 'certain' – where a contact is directly observed. Surficial units are denoted with shades of black and grey with no separate boundary symbology and textural overlays are denoted by black patterned areas. For familiarity global elevation uses a 'MOLA like' colour scales whilst a divergent scale in muted tones is used locally to highlight topographic differences.

2.2.4. Measurements

When the map sheet was complete, cross sections and summary scientific publications were produced. To aid the cross-section and unit descriptions several measurement of 'unit thickness have been made. These measurements have been made using the mean difference in 10 pairs of spot hights collected at the shortest path across the unit margin whist considering the quality of the underlying DTM and should be only considered estimates of the apparent thickness.

3. Results

The main map (CTX DEM and ORI mosaics) (Figure 3) covers 8750 km^2, spans an elevations range of ~ 600 m, and from −2992 m in the Aquitania region to the SE to −3156 m at the base of a crater floor in thePannonia region to the NW the mean eleevation is -3077 m with a standerd devation of 35 m. The map consists of 15 bedrock units organised into 6 groups, 7 textural and surficial units (see Description Of Map Units (DOMU): Table 4) and structural interpretations. The bedrock units represent geological processes dating back to the mid-Noachian. Our interpretation of the stratigraphic relationships, and their relative timing relative to other regional aqueous, erosional, and tectonic processes is shown in the Correlation Of Map Units (COMU) diagram (Figure 3). These relationships and their significance will be detailed in a future publication on the Geological history of Oxia Planum.

4. Discussion

4.1. The discrimination between units and key stratigraphic relationships

This map is a detailed investigation into geological units in Oxia Planum that will support exploration with the Rosalind Franklin rover. The spatial constraints of the study area, dictated by the mapping scale required to fulfil the objective of the map, relative to the size of geological features in the region mean that the map cannot cover a sufficiently large extension to formulate complete hypotheses. To

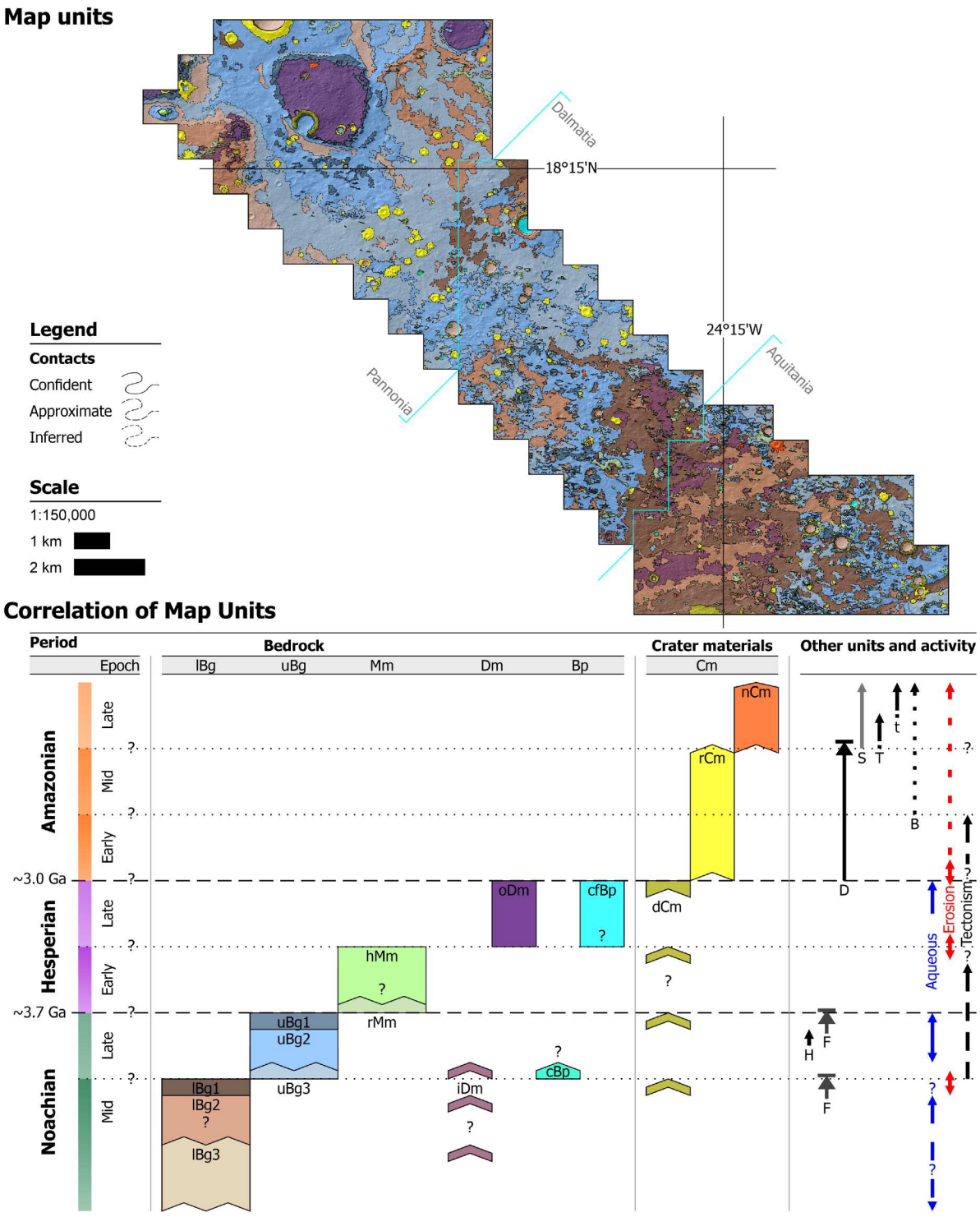

Figure 3. The map of rock units and correlation of map units. The 1:150,000 scale map of bedrock units from the main map and the correlation of map units (Skinner et al., 2022). The timing of events is drawn from the contextual geological literature and the timing of other events in the region (e.g. Sections 1.2 & 4.2). Coloured bars represent the time in which these events are likely to have occurred, and not representative to their duration. We have not derived impact crater size frequency distribution model ages of for map units because, following the discussion in Sun and Stack (2020), these techniques is not an appropriate technique for units of this size and in this complex state of erosion/exhumation (e.g. Warner et al., 2015).

address this challenge, we have defined units with enough high fidelity to aid exploration and be representative of the wider Oxia Planum region. Here we outline these decisions in stratigraphic order and discuss open questions presenting avenues for further exploration.

4.1.1. Bedrock units

In the lower bedrock group (lBg) we map three units, all strongly associated with spectral signatures of aqueous alteration. We chose to be generous in retaining division between the units in the lower bedrock group to identify where differences in the expression of the

Table 4. Description of map units.

Unit	Unit name – Description HiRISE & CaSSIS (Near Pan and Blue; NPB)	Additional information (Unit associations, other details, compositional information)	Interpretation and Hypotheses of superposition and emplacement	Examples CaSSIS (1:10,000) and HiRISE (1:2000) examples
B	Boulders – HiRISE: Isolated dark blocks that often cast shadows. Distribution identified by NOAH-H (e.g.; Barrett et al., 2022). CaSSIS: Below resolution.	Associated with oDm, and impact craters (nCm, rCm). There are no resolvable compositional associations.	Overlies all other units. Common throughout the region in similar contexts associated with Dark material and recent impact craters.	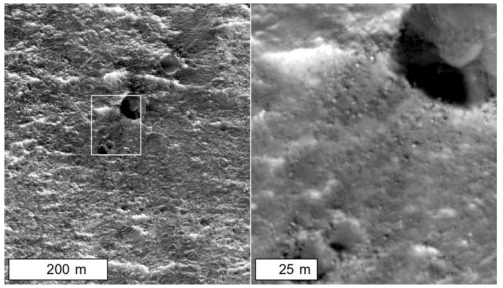
t	**TAR field –** HiRISE: Dark toned smooth mantling material with numerous small (<1 m) ripples. CaSSIS: Blue tones with low relief.	Numerous small (<5 m wavelength) ripples that make the bedrock identification challenging. Mafic or blank spectral signatures.	Overlies other units and are closely associated with units T and S. Common throughout the region particularly in lower elevations towards Chryse Planitia.	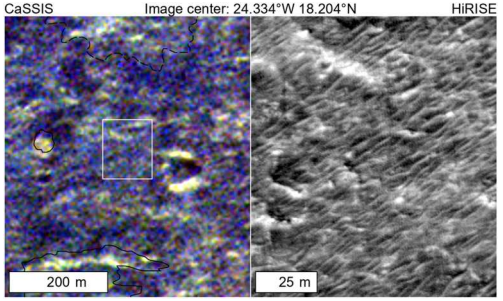
T	**Large TARs –** HiRISE: Bright faced elongated ridges. CaSSIS: High relief, high albedo ridges with orange tones on illuminated slopes.	Often found in topographic lows (e.g. crater floors) or channels. Ridges are resolvable in DEM data. No clear compositional signature (Berman et al., 2018).	Overlies other units as isolated TAR's or grades into smaller continuous, often lower relief, TAR fields (e.g. t). Found in similar contexts throughout the region and strongly associated with sediment fan remnants in Ratia Palus.	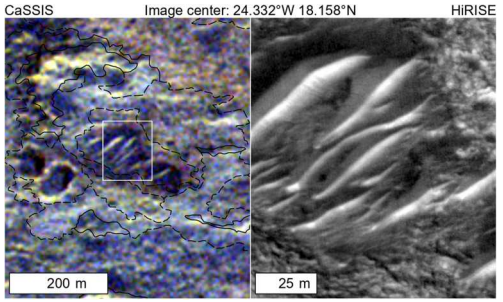

(*Continued*)

Table 4. Continued.

Unit	Unit name – Description HiRISE & CaSSIS (Near Pan and Blue; NPB)	Additional information (Unit associations, other details, compositional information)	Interpretation and Hypotheses of superposition and emplacement	Examples CaSSIS (1:10,000) and HiRISE (1:2000) examples
S	**Smooth material –** HiRISE: Mid toned, smooth, mantling material. CaSSIS: Blue tones with low relief.	Occasional aeolian ripples superposed. Smooth margins. Often found in recent impact craters or expressed as loose material on scarps. Mafic or spectrally blank signatures.	Overlies other units and closely associated with unit t. Common throughout the regions where loose material accumulates in local topographic lows.	
D	**Dark patches** – HiRISE: Smooth mid to dark toned material. CaSSIS: Dark blue with low relief.	The unit is bounded by small scarps (<1 m high). There is some association with ripples (surface can be 'wavy'). No resolvable compositional associations.	Unconformably overlies bedrock units. Located in local topographic lows. Patches are progressively more dissected from SE-NW. Regionally they are found close to recent impact craters.	
F	**Widely spaced fractures –** HiRISE: Polygonal to rectilinear troughs ~1–5 m wide with spacings of 10 m – 20 m. CaSSIS: Dark lineations in other units.	No resolvable compositional associations.	Predominantly occur in association with uBg1 and lBg1. Common throughout the region in similar contexts.	

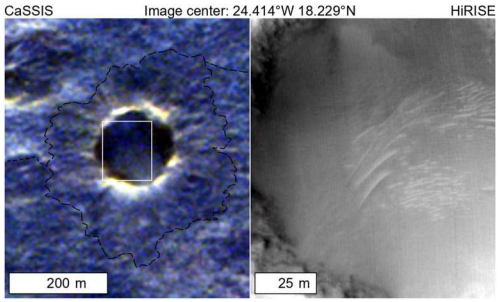

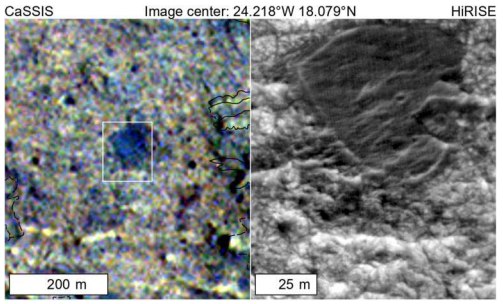

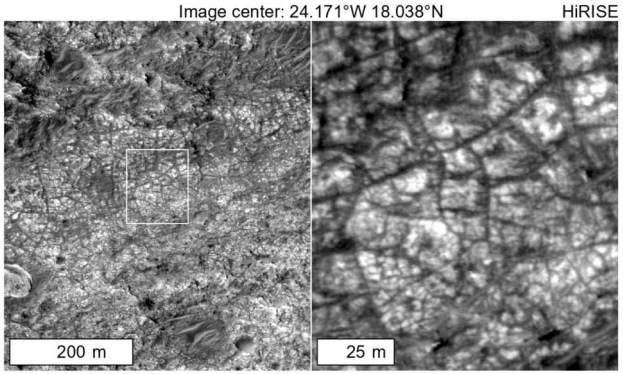

H	**Honeycomb** – HiRISE: Polygonal to rectilinear ridges ~2 m wide with spacings of 10 m – 20 m. CaSSIS: Below resolution.	Often highlighted by smooth dark material between the ridges. No resolvable compositional associations.	Predominantly occurs in local topographic highs of uBg2, under uBg1, and around mesas capped with oDm.

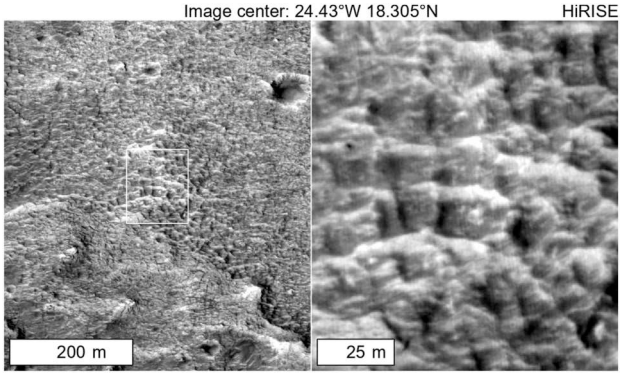

Ejecta material group

nCm	**New crater material –** HiRISE: Very dark halo around small circular pits. CaSSIS: Very dark/black.	Continuous ejecta. ~2–3 crater radii from the crater with diffuse margins that fade into the surrounding units. No resolvable compositional associations.	Overlies all other units and associated with boulders. Randomly distributed and not related to any specific geologic unit.

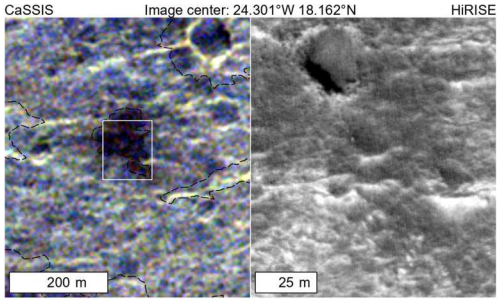

rCm	**Recent crater material –** HiRISE: Smooth mid to dark toned material with moderate relief. Structure is radial to a local topographic low (i.e. something confidently identified as an impact crater). CaSSIS: Very dark/black.	Diffuse margin between the ejecta and the surrounding units. No resolvable compositional associations.	Occasionally superposed by surficial group units. Randomly distributed and not related to specific geologic unit.

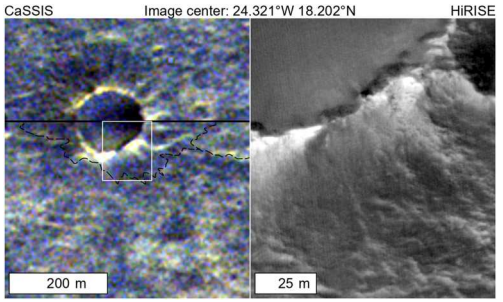

(*Continued*)

Table 4. Continued.

Unit	Unit name – Description HiRISE & CaSSIS (Near Pan and Blue; NPB)	Additional information (Unit associations, other details, compositional information)	Interpretation and Hypotheses of superposition and emplacement	Examples CaSSIS (1:10,000) and HiRISE (1:2000) examples
dCm	**Degraded crater material –** HiRISE; High relief, often with diffuse margins or found on local topographic highs. CaSSIS; Variable, dark blue/orange with yellow toned highlights.	Crater rims removed and little or no ejecta remains. No resolvable compositional associations.	Can be superposed by S, Mm and uBg units. Randomly distributed and not related to specific geologic unit.	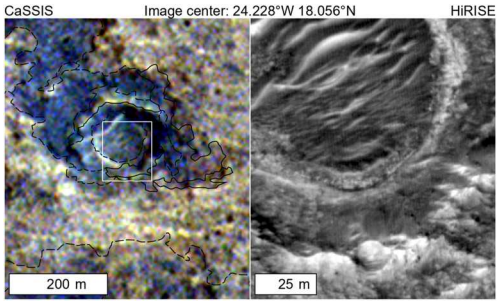
Dark group				
oDm	**Overlying dark material –** HiRISE: Dark-toned, rough, boulder-forming ridges with dark smooth troughs. CaSSIS: Predominantly blue tones with small, dark blue zones.	Located on local topographic highs. The unit's margin is recessed from the tops of scarps and it is sufficiently thin (~ 1 m) to contain occasional windows into underlying lighter toned units. CRISM pyroxene signatures (Quantin-Nataf et al., 2021) and possible weak phyllosilicate signatures.	Appears to unconformably overlie F in unit uBg1. Found in regional topographic lows, on local topographic highs, often surrounded by a moat. Often found in continuum with inverted and low relief channels (Davis et al., 2023; Fawdon et al., 2022).	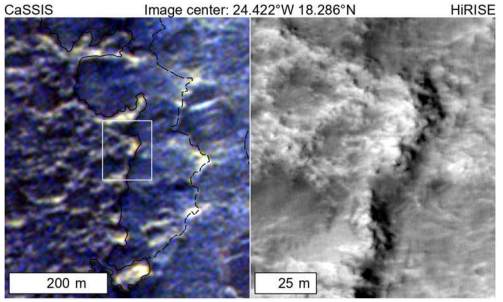
iDm	**Interbedded dark material –** HiRISE: High relief, bright ~1–3 m diameter rounded knobs picked out by dark infilling material. Occasional bright blocks. CaSSIS: Dark or mottled because the bright knobs are often below the CaSSIS resolution, whereas the unit is lower relief, bright purple-orange tones.	Located in local topographic lows. Appears to crop out in erosional windows within bedrock units. No phyllosilicate signatures observed.	This unit appears to occur sporadically and be interbedded with lBg2. Similar examples of this material are seen occasionally across the region.	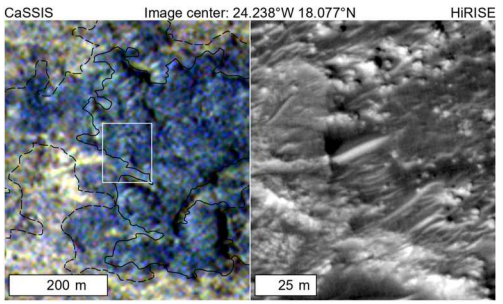

Bright group				
cfBp	**Crater fill bright patches –** HiRISE: Mid to bright toned, low relief with concentric dark lineation. CaSSIS: Bright/white tones.	Located within degraded impact craters > ~150 m. No observed compositional relationships.	Strongly associated with dCm. Overlain by surficial units. Not seen to be overlain by other units. Common throughout the region in degraded impact craters > 150 m in size. It is not seen to be overlain by anything other than surficial units.	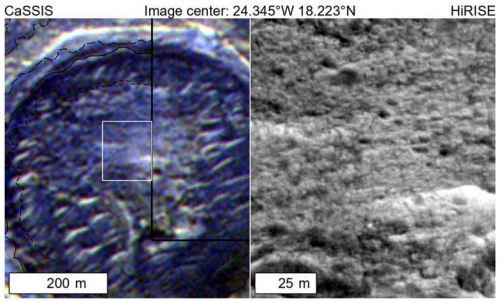
cBp	**Concentric bright patches –** HiRISE: Mid to bright toned, low relief with distinct concentric dark lineation. CaSSIS: Bright/white tones contrasting to subjacent bluer tones.	Located in local topographic lows with distinct marginal steps No observed compositional relationships.	Overlies lBg units. The moat around the edge often hosts aeolian material. Not seen in association with uBg units and occasionally overlain by rMm. Common thoughout the region where the orange toned material is exposed. Regional observations suggest cBp is superposed by material from the uBg, and Mm unit groups (McNeil et al., 2022).	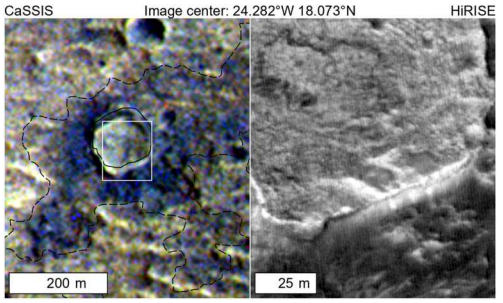
Mound group				
hMm	**Hill mound material –** HiRISE: Smooth, bright, conical mounds ~100 m across and up to 10 m in height. The bright smooth surface has occasional lineations. CaSSIS: Yellow tones in all illumination angles.	hMm forms the tops of larger mounds. Mounds often have a bright layer half way up, scree around their bases and occasionally have small impacts on them. No good CRISM observations are avaliable in Oxia Planum.	Directly overlies uBg1 with uBg2 and uBg3 forming the base of the topographic mound below hMm. hMm never overlies oDm. Mounds with hMm are part of a population extending 100s of km into Chryse Planitia (McNeil et al., 2022). In Oxia Planum hMm must predate oDm. Some mounds are dissected by troughs and have internal ridges.	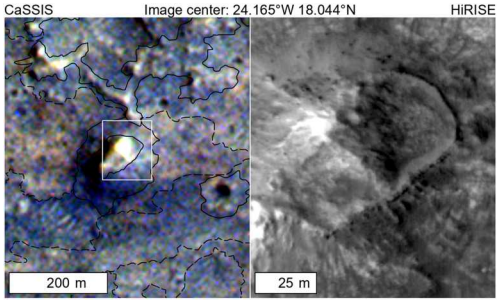

(*Continued*)

Table 4. Continued.

Unit	Unit name – Description HiRISE & CaSSIS (Near Pan and Blue; NPB)	Additional information (Unit associations, other details, compositional information)	Interpretation and Hypotheses of superposition and emplacement	Examples CaSSIS (1:10,000) and HiRISE (1:2000) examples
rMm	**Ridge mound material** – HiRISE; Bright upstanding knobby patches and ridges often with a dark unconformity (contact?) seen at base. CaSSIS; High relief, yellow toned.	Bright 'knobbles' often trend into ridges parallel to the trend of periodic bedrock ridges (PBRs). No resolvable compositional associations.	Knobbles and ridges both overlie uBg and lBg group. Similar ridges are frequently seen thoughout the wider Oxia Planum region commonly trend into PBRs (Favaro et al., 2021).	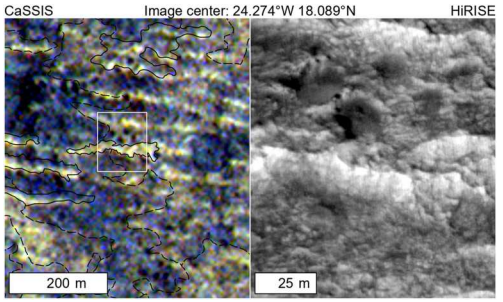
Upper bedrock group				
uBg1	**Upper Bedrock Group 1 –** HiRISE: Mid to bright toned, low relief, smooth with widely spaced (>5 m) fractures forming a crisply-defined layer ~1 m thick. CaSSIS: Low relief, bright/white/grey tones.	Strongly associated with the top of local topographic highs and scarps. Not strongly associated with phyllosilicate minerals in CRISM.	Overlies uBg2 It is overlain by examples of both the Mm and Dm groups. Similar units appear at the top of scarps and on local topographic highs throughout the region where they are often overlain by Mm and Dm group style units.	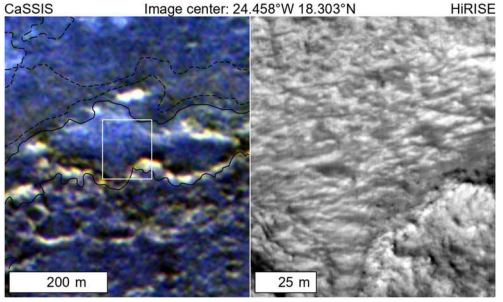
uBg2	**Upper Bedrock Group 2 –** HiRISE; High relief, bright, rugged material, forming low hills. CaSSIS: High relief with bright/blue tones.	Forms wide (>100 m) upstanding areas in all regions of the map. Strongly associated with the 'honeycomb' texture and scarps in Pannonia. Some association with phyllosilicate minerals and possible mixtures with olivine (Mandon et al., 2021). Dark regolith distribution below the CRISM pixel size may obscure this signal.	Overlies or grades downwards into uBg3, low hills of this unit are often capped with uBg1. Directly underlies uBg1 in mesa walls. Occurs thoughout the Oxia Planum region. Crater wall cross-sections show sedimentary architecture. Layering often variable in thickness. uBG1 is also strongly associated with inverted/exhumed channels (Davis et al., 2023)	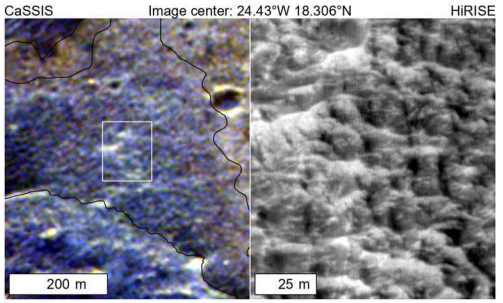

uBg3	**Upper Bedrock Group 3 –** HiRISE: Bright, rough, small-scale (<5 m) fractures/knobs with darker material between them. CaSSIS: Dark blue/black with bright speckles.	Small patches of S t and D material frequently overlie the surface complicating identification. Not sampled in any CRISM data.	Occurring as a layer around the bottom of larger mesas of uBg2 and appears to underly uBg2. Appearing as outliers overlying lBg units. Evident in the stumps at the base of rounded buttes capped with hMm where HiRISE coverage permits observation.	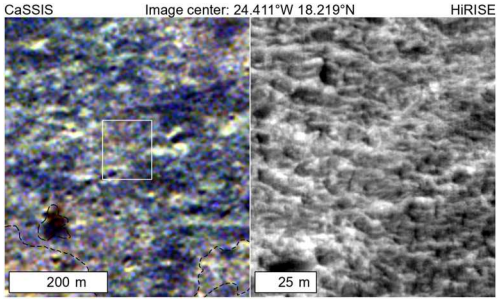
Lower bedrock group				
lBg1	**Lower Bedrock Group 1 –** HiRISE: Bright, low relief, smooth surface with widely (>10 m) spaced fractures picked out by dark material. CaSSIS: Low relief with light orange to cream tones.	The boundary with lBg2 appears gradational but anaglyphs suggest a layered structure. Strong spatial correlation with phyllosilicate spectral signatures.	Directly underlies uBg units and cBp and has a gradational boundary with lBg3. Across the Oxia Planum region, material similar to lBg1 crops out below uBg-style material where it consistently correlates with phyllosilicate spectral signatures. Also spatially correlates with PBRs.	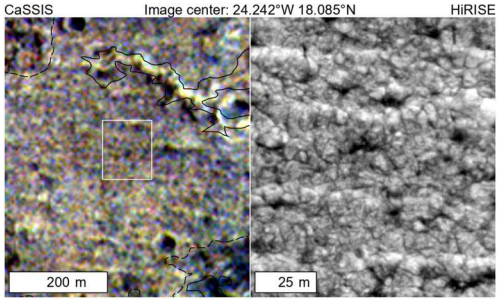
lBg2	**Lower Bedrock Group 2 –** HiRISE: Bright, low relief surface with wide (>10 m) spaced fractures and ridges highlighted by dark infill. CaSSIS: Low relief with dark orange/grey and bright white tone.	Often occurs in slightly lower, rougher areas than adjacent lBg1. The more eroded fractures have more dark infill. Below the resolution of CRISM observations.	There is a gradational boundary with lBg1 but a distinct topographic step (~50 cm) between the two where iDm is exposed. Seen throughout the wider Oxia Planum where scarps or windows though lBg allow.	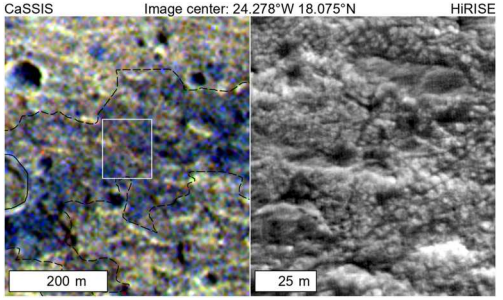

(*Continued*)

Table 4. Continued.

Unit	Unit name – Description HiRISE & CaSSIS (Near Pan and Blue; NPB)	Additional information (Unit associations, other details, compositional information)	Interpretation and Hypotheses of superposition and emplacement	Examples CaSSIS (1:10,000) and HiRISE (1:2000) examples
lBg3	Lower Bedrock Group 3 – HiRISE: Bright, low relief surface with moderately (~5–10 m) spaced fractures that show no strong orientation pattern. CaSSIS: Low relief with bright, light orange tone.	Only seen at the lowest elevations of the map (Pannonia and impact craters). The margins can appear to grade into the other surrounding units. Very strong spatial correlation with phyllosilicate spectral signatures.	It could underlie or be at the same level as examples of iDm. Elsewhere in the region this unit often occurs in areas with bright orange tone in CaSSIS data, and occur in the lowest parts of the topography.	

Note: Description of map units organised from youngest to oldest as on the Main Map.

unit exist. Significant differences in expression include variations in fracturing and layering seen throughout the group (lBg1 – lBg3) and Brighter materials (lBg2) having a larger amount of dark regolith trapped in their 'knobby' texture. Only in a few instances are these textural variations clear and it remains an open question as to whether they represent stratigraphically distinct lithologies or lateral variation in preservation and erosion processes, or both. Nevertheless, these mapped contacts are locations to investigate potential lithological variation – , even if the actual significance of these divisions is currently unclear.

In the upper bedrock group (uBg) we also map three units. The uBg dose not have such a strong association with aqueous alteration, but in the wider Oxia Planum region do contain exhumed fluvial channel bodies (Davis et al., 2023; Fawdon et al., 2022). The top of the group (uBg1) forms a thin resistant layer directly underlying both the Mound material group and the overlying Dark material unit. The thin resistant layer is separated from the rest of the group to document the extent of this possible paleo-surface and because the other units (uBg2,3) host a boxwork of upstanding ridges (H) which we interpret to probably be inverted mineralised fractures, which in turn could represent phases groundwater activity of great interest to the mission (e.g.; Kronyak et al., 2019).

We map two units in the Mound material (Mm) group. These units constitute isolated hills (hMm) that make up the lithologically distinct top parts of geomorphological identifiable mounds. These landforms are thought to be remnants of a ~100 m thick layer (McNeil et al., 2022). However, the deposition and erosion mechanisms for the unit, which may be significant for the preservation of biosignatures, are unresolved. Ridge mound material (rMm) is included separately because it was not always clear if these small outcrops, which appear similar to the top of the mounds, always have a contact at their base or are ridges in other units and an artefact of illumination.

The Dark material (Dm) in the mapping area are found to occurred in two circumstances and are mapped as two units. At the top of the stratigraphy the overlying dark material (oDm) unit is thin (~<5 m), is rough in textured, contains abundant trapped loose material trapped in its surface. oDm occurs at on local topographic highs (such as inverted craters and channels), or in regional topographic lows surrounded by a shallow moat meaning that it is still at the top of the stratigraphy. Regionally dark material in these settings are associated with fluvial systems (Fawdon et al., 2022) and mafic spectral signatures (Quantin-Nataf et al., 2021). However, a type of dark material is also found within erosional windows and appears to be interbedded with the lBg. Dark material in this setting often appears to be dark sand around bright blocks but the reason for this roughness with

respect to the low relief surrounding units is unknown. This 'Dark material' would substantially predate the overlying Dark material (oDm) thus we discriminate to aid future investigation identifying interbedded Dark material (iDm) units.

Light-toned patches with concentric layers occur in two distinct settings. Concentric bright patches (cBp) occur in small (<100 m) relic impact structures predominantly overlying the lower bedrock group (lBg1). Whilst these may be contemporaneous with the base of the upper bedrock group (Ubg3), their distinct setting and appearance suggests a localised process warranting their distribution be mapped separately. Crater infill bright patches (cfBp) appear similar to cBp but occur within larger (>250 m) craters with well defined rims. Consequently, this crater fill (cfBp) material must substantially post-date the craters themselves and when the upper bedrock group in the craters formed. However, all these light toned patches may have formed at the same time if cBp represents erosional remnants of a process that is simply better preserved as cfBb in the larger craters. These units are mapped separately to avoid interpretive stratigraphic assumptions.

Impact Crater materials (Cm) have been mapped based on three classes of degradation. Craters with the best preserved morphology (nCm) are recorded to identify relatively recent impacts that have occurred, and exposed fresh bedrock. Other crater materials are divided into recent (rCm), where there is not significant reworking of the crater or ejecta, and degraded examples (dCm) that we consider to be older. This class (dCm) records the parts of impact structures associated with impact lithologies (ejecta remnants, disaggregated rims) but other bedrock lithologies, exposed by the impact process, when also visible, are mapped with those stratigraphically appropriate units.

4.1.2. Surficial units

Five surficial units and two texture overlays represent units that crop out discontinuously across the region, deposits of mobile material, and surface patterns that transcend several other units. The Dark (D) and Smooth (S) surficial units are found intermittently across the mapping area. The Dark unit is notable in that it often exhibits a 'stepped' edge, which indicates a degree of induration that is not seen in the Smooth unit (S), which in turn represents what is likely to be unconsolidated material, such as scree at the foot of scarps. Boulders (B) and two classes of aeolian bedforms (T and t) were mapped based mainly on their identification in the NOAH-H data set (Barrett et al., 2023). These units were mapped to help understand the modern aeolian environment (E. A. Favaro et al., 2021) and also because understanding the distribution of these bedforms is vital when considering rover locomotion for long term planning. Finally, the Honeycomb (H) and Fracture (F) textures observed across several units representing specific processes and events associated with their geological history. These are recorded to indicate their distribution for future study, as they may be related to possible paleo-surfaces, regional stress fields, or host resistant fracture-fills indicative of ground water activity and may be therefore relevant to the objectives of the rover mission (e.g. Vago et al., 2017).

4.1.3. Structural observations

Three classes of structural observation are recorded on the map. Three probable reverse fault zones are inferred in the Pannonia region. This inference is drawn from the pattern of repeated UGB and LBG units, the topographic break in slope and that the spacing of these features is consistent with the strike scale and spacing of shortening structures in the region (e.g.; Woodley et al., 2023). The 54 lineaments represent a variety of linear features including fractures, 10's–100's m long which the stratigraphy. These may represent faults, but no clear evidence of displacement is seen. We also observed polygonal to rectilinear fractures through to relate to the region tectonic fabric (e.g.; Apuzzo et al., 2021). These recorded as a textural overlay and described with the units in which they occur (Table 4).

4.2. Relationship to previous mapping

Previous mapping efforts have focused on many different aspects of Oxia Planum (Figure 4) with regional studies (Ivanov et al., 2020; Tanaka et al., 2014), spectroscopic studies (Brossier et al., 2022; Gary-Bicas & Rogers, 2021; Mandon et al., 2021; Parkes-Bowen et al., 2022), and terrain characterisation works (Mastropietro, 2019) investigating the geological history (Quantin-Nataf et al., 2021; Uthus, 2020) and the proposed landing area. Where these maps overlap the area of this work, a variety of 'clay bearing' or 'light toned' plains units (e.g. CBP) are identified cropping out over the majority of the area mapped, as well as instances of a 'dark capping or resistant units' (e.g. DRU) and examples of 'isolated mounds' are mapped.

Exploration of the CBP has used hyperspectral (CRISM; Brossier et al., 2022; Mandon et al., 2021) and multispectral (THEMIS; Gary-Bicas & Rogers, 2021; CaSSIS; Parkes-Bowen et al., 2022) data supported by HiRISE. Mandon et al. (2021) identified 'Orange' and 'Blue' spectral classes, with their distribution and relationship to fracture patterns mapped by Parkes-Bowen et al. (2022). These classes loosely relate to units in our upper Bedrock (blue, uBg) and lower Bedrock (orange, lBg) groups, but should never be taken as a direct correspondence

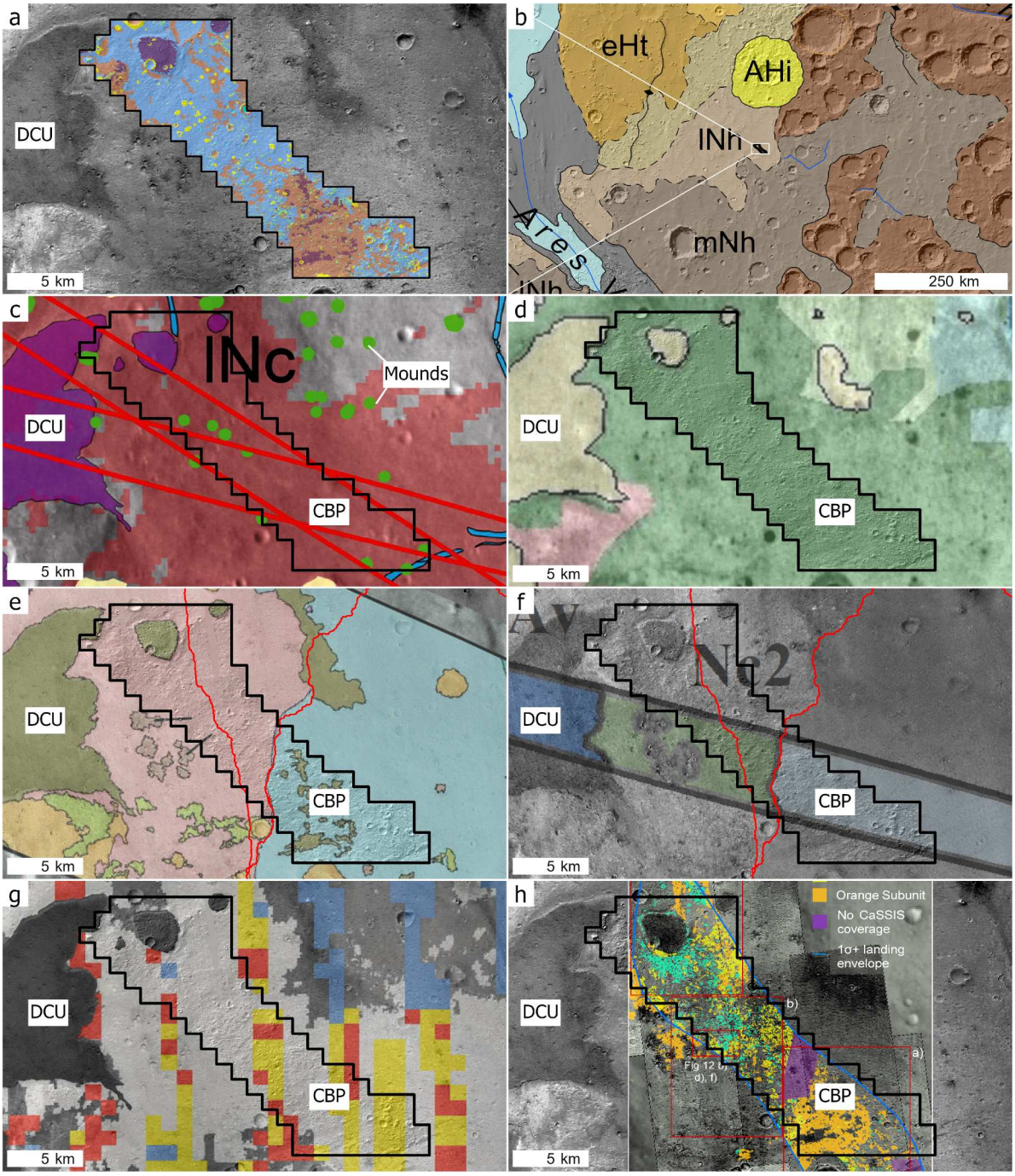

Figure 4. Relationship to previous mapping. A comparison between this and previously published maps covering Oxia Planum. (a) Simplified version of this map. (b) Context from the global geological map showing that our study area lies in a Late-Noachian highland (lNh) unit (for other labels see Tanaka et al., 2014). (c) Preliminary mapping from Quantin-Nataf et al. (2021) established the key regional units including the 'Clay-Bearing Plains' (CBP) and 'Dark Capping Units' (DCU) and the mounds. (d) Uthus (2020) mapped the CBP as one unit, but (e) Ivanov et al. (2020) and (f) Mastropietro (2019) divided this unit in the middle of our study area. Inspection of this boundary shows that it is a mosaicking artefact seam lines from The Murry Lab (2023) Beta release (shown in red), not a real geological boundary. (g) Mandon et al. (2021) split the CBP into different classes using HiRISE and CRISM to identify 'orange' and 'blue' sub-units, the distribution of which are shown mapped in (h) by Parkes-Bowen et al. (2022). For full description of each map see the respective publications.

because our mapping used much higher resolution data and considers geological context independently of interpretation of mineralogical inferences from spectroscopy. Other mapping efforts either did not attempt to differentiate the CBP (e.g. Ivanov et al., 2020; Mastropietro, 2019; Uthus, 2020) at their mapping scale, or the authors divide the CBP based on an erroneous observation of an apparent albedo difference made using the beta release of the Murray lab global CTX mosaic that is, in actuality, a mosaicking artefact with no geological significance – later corrected in the full data release (The Murry Lab, 2023).

There is a good correlation between the DRU of previous works and the Overlying Dark Material

(oDm) units. This map and these works did not have sufficient resolution to record what we identify as the interbedded Dark material or that the DRU is only a very thin (<5 m) layer and recessive compared to the subjacent material (uBg3) which forms the cliff edges of the mesas. There is also a direct correlation between the 'mounds' of Quantin-Nataf et al. (2021), the Mound Material group from this study, and a detailed regional investigation of these landforms (e.g. McNeil et al., 2021).

4.3. Anticipated use in rover operations

The purpose of this map is to inform the ExoMars rover mission. The map creates a connection between planning for the rover's traverse and regional geological context and we anticipate that it will be used throughout the envisaged reference surface mission (Vago et al., 2017).

After Entry Descent and Landing (EDL), the rover will carry out a 15-day commissioning phase which will include rover deployment, egress, moving away from the lander, and commissioning the rover subsystems, the instruments, and the rover's analytical laboratory chemical background. During this time, we will conduct a validation exercise, connecting the initial PanCam panorama to our mapped geological units. After considering this 'calibration' we will use the map to inform the initial direction taken by the rover. In the case that the landing site is not within the mapped area, then a rapid reconnaissance mapping protocol (Section 2.2) would be implemented as successfully tested for an ExoMars like mission scenario by Balme et al. (2019).

Following commissioning, the mission will consist of a number of traverses and the exploration of various locales. Six experiment cycles (each including drives, identification of prime targets and near surface plus subsurface samplings) and two deep vertical surveys (where at a single location samples are obtained and analysed at 50 cm depth intervals) are planned for the nominal mission. To support this, we use the map to establish a suite of visual hypotheses; that is, the map creates a framework showing us where we can go to investigate different aspects of the regional geology, and what types of questions can be answered at each location. For example, the map shows us where we can ask 'what is the lithology of the upper bedrock group', and then provides a guide for where to move the rover to investigate follow up questions such as 'does the lithology of the upper Bedrock group become more conducive to the preservation of organic material as we go down section?' The map will connect the rover observations made in these locales with our understanding of the spatial and stratigraphic distribution of geological units and allow us to gradually construct a thorough understanding of the paleoenvironment. This understanding of geological context is critical to correctly choose where to conduct experiment cycles and especially the resource-hungry vertical surveys. The end goal is to maximise our chances of collecting samples that may possess diagnostic chemical biomarkers in a good state of preservation.

Finally, the map will be used for long term strategic planning and team communication. If the mapped unit prove to be meaningful, we anticipate that that long terms plan would attempt to explore, or sample, each of the major bedrock groups and detailed hypotheses relating to each of these groups will subject of future companion publications. By making the map available though MMGIS (Calef et al., 2017) planned long-term drive targets, strategically planned traverse routes, and the daily location of the Rosalind Franklin can be displayed together. In MMGIS, the wider team will be able to interact with the strategic decision-making progress and appreciate how the rover sits within the geologic context. By enabling team access to this information, strategic decision-making will be more robust, inclusive, and should lead to more efficient and productive mission progress.

4.4. Outlook

This map represents a key part of the ongoing study of Oxia Planum in preparation for the ExoMars rover mission. In addition to usage outlined above the units and observations are applicable to the Oxia Planum region and – using observation from the region beyond the mapping area, are the basis for more general investigation into the geological history of the region. This will identify of hypotheses for the origin of each units that can be evaluated by Rosalind Franklin. The map and associated data will be used in detailed studies. Such as semi-autonomous terrain classification in the Oxia region or quantitative evaluation of 3D geometry of the mapped units. Finaly this map will be a guide for spectroscopic studies ground truthing CRISM hyper- and CaSSIS multi- spectral data with the PanCam (Coates et al., 2017; Cousins et al., 2012), Enfys (Gunn, 2023), MaMISS (De Sanctis et al., 2017) and μOMEGA (Bibring et al., 2017) instruments on the ExoMars rover and also serve as example for future mission planning.

5. Conclusions

We have created a high resolution geological/morpho-stratigraphic map of the ExoMars Rosalind Franklin rover landing site in Oxia Planum. The map is presented at a scale of 1:30,000 but digitisation was performed at a scale of 1:2000, a scale relevant to rover operations. Digital version of the map are available (Fawdon et al., 2023). To create the map, we used a

two-phase process of group mapping followed by expert reconciliation. The mapping exercise has provided the wider ExoMars rover team with a sound knowledge of the landing site and has also helped us to develop new geological hypotheses for the region. As a summary of spatially located geological hypotheses, the map will be used to guide rover exploration and, when these hypotheses are tested with surface observations, will enable the team to identify suitable locations for sample acquisition using the rover's drill system, and hence improve the chances of the mission meeting its search for life goals. In addition, the map provides the geological framework necessary to provide context for these samples, such that any important discoveries can be tied into the Mars' regional and global geological record.

Software

The map and other datasets were created and compiled in ESRI ArcPro 2.9–3.1. Individual HiRISE Digital Elevation Models were created in SocetSet® and Integrated Software for Images and Spectrometers (ISIS3). Creation of the CaSSIS RGB products was completed using ISIS3. Georeferencing was conducted in ESRI ArcPro 2.9–3.1. The HiRISE orthomosaic and DEM basemap (Volat & Quantan-Nataf, 2020) was produced using the MarsSI infrastructure (Quantin-Nataf et al., 2018 The data collection in the concurrent team mapping used Multi-Mission Geographic Information System (Calef & Soliman 2019).

Acknowledgements

The ExoMars Rosalind Franklin Mission is a partnership between ESA and NASA. The Rosalind Franklin Rover has eight instruments in its 'Pasteur' Payload, with Principal Investigators from seven countries all of whom we would like to thank for there support of this project. We would like to acknowledge the following funding bodies, people and institutions supporting the lead authors of this work. We thank the UK Space Agency (UK SA) for funding P. Fawdon, on grants; ST/W002736/1, ST/L00643X/1 and ST/R001413/1, MRB on grants; ST/T002913/1, ST/V001965/1, ST/R001383/1, ST/R001413/1, P. Grindrod on grants; ST/L006456/1, ST/R002355/1, ST/V002678/1 and J. Davis on grants ST/K502388/1, ST/R002355/1, ST/V002678/1 through the ongoing Aurora space exploration programme. C. Orgel was supported by the ESA Research Fellowship Program. Alessandro Frigeri: was funded by the Italian Space Agency (ASI) grant ASI-INAF number 2017-412-H.0 (ExoMars/Ma_MISS) and D. Loizeau was funded by the H2020-COMPET-2015 programme (grant 687302), C. Quantin-Nataf was supported by the French space agency CNES, I. Torres was supported by an ESA Young Graduate Traineeship, A. Nass was supported by Helmholtz Metadata Projects (#ZT-I-PF-3-008). We thank NASA and the HiRISE camera team for data collection support throughout the ExoMars landing site selection and charectorisation process. The USGS for the HiRISE DTM data and maintaining the ISIS and SOCET SET DEM workflows. The authors wish to thank the CaSSIS spacecraft and instrument engineering teams. CaSSIS is a project of the University of Bern and funded through the Swiss Space Office via ESA's PRODEX programme. The instrument hardware development was also supported by the Italian Space Agency (ASI) (ASI-INAF agreement no. I/2020-17-HH.0), INAF/Astronomical Observatory of Padova, and the Space Research Center (CBK) in Warsaw. Support from SGF (Budapest), the University of Arizona (Lunar and Planetary Lab.) and NASA are also gratefully acknowledged. Operations support from the UK Space Agency under grant ST/R003025/1 is also acknowledged. This research has made use of the USGS Integrated Software for Imagers and Spectrometers (ISIS) Technical support for setup of the Multi-Mission Geographic Information System for concurrent team mapping was provided by F. Calef (III) and T. Soliman at NASA JPL and S. de Witte at ESA-ESTEC.

Disclosure statement

No potential conflict of interest was reported by the author(s).

Funding

This work was supported by Agencia Estatal de Investigación [grant number ID2019-107442RB-C32, MDM-2017-0737]; Agenzia Spaziale Italiana [grant number 2017-412-H.0]; Bundesministerium für Wirtschaft und Technologie [grant number 50 QX 2002]; Centre National de la Recherche Scientifique; Centre National d'Etudes Spatiales; Euskal Herriko Unibertsitatea [grant number PES21/88]; Istituto Nazionale di Astrofisica [grant number I/ 060/10/0]; Ministerio de Economía y Competitividad [grant number PID2019-104205GB-C21]; Ministry of Science and Higher Education of the Russian Federation [grant number AAAA-A18-118012290370-6]; National Aeronautics and Space Administration [grant number NNX15AH46G]; Norges Forskningsråd [grant number 223272]; European Union's Horizon 2020 (H2020-COMPET-2015) [grant number 687302 (PTAL)]; Sofja Kovalevskaja Award of the Alexander von Humboldt Foundation; MINECO [grant number PID2019-107442RB-C32]; The Open University [grant number Space Strategic Research Area]; European Union's Horizon 2020 research and innovation programme [grant number 776276]; H2020-COMPET-2015 [grant number 687302]; The Research Council of Norway, Centres of Excellence funding scheme [grant number 223272]; Helmholtz Metadata Projects [grant number ZT-I-PF-3-008]; The Research Council of Norway [grant number 223272]; Swiss Space Office via ESA's PRODEX programme; Ines Torres was supported by an ESA Young Graduate Traineeship; Schweizerischer Nationalfonds zur Förderung der Wissenschaftlichen Forschung [grant number 200021_197293]; Science and Technology Facilities Council [grant number 1967420]; UK Space Agency [grant number ST/K502388/1, ST/R002355/1, ST/V002678/1].

Data availability statement

The data used in the map, the informal geographic areas, the rover operations quad grid, and the multiband CaSSIS cubes being used for the scientific evaluation of Oxia Planum are freely available through the ESA Guest Storage Facility

(https://www.cosmos.esa.int/web/psa/exomars2022-rsowg_oxia-planum_geography-cassis-ctx_v1.0) and as the supplementary data set to (Fawdon et al., 2021). The map geodatabase is available through The Open University (Fawdon et al., 2023) The HiRISE orthomosaic and DEM (Quantin-Nataf et al., 2018; Volat & Quantan-Nataf, 2020) basemap was produced using the MarsSI infrastructure, is published on the Planetary SUrface Portal (PSUP), and is co-registered with the datasets presented here. Individual HiRISE DTM are being released publicly through the University of Arizona (Table 1). NOAH-H data and HiRISE basemap information is available through Barrett et al. (2023). A package of the map layers including georeferenced HiRISE RGB data is publicly available through the ArcOnline living atlas https://arcg.is/0y4bSa.

ORCID

Peter Fawdon http://orcid.org/0000-0003-1900-8347
Csilla Orgel http://orcid.org/0000-0001-7317-0092
Solmaz Adeli http://orcid.org/0000-0001-9972-409X
Matt Balme http://orcid.org/0000-0001-5871-7475
Fred J. Calef http://orcid.org/0000-0002-5132-3980
Joel M. Davis http://orcid.org/0000-0003-3522-7910
Alessandro Frigeri http://orcid.org/0000-0002-9140-3977
Peter Grindrod http://orcid.org/0000-0002-0934-5131
Ernst Hauber http://orcid.org/0000-0002-1375-304X
Laetitia Le Deit http://orcid.org/0000-0003-1361-5170
Damien Loizeau http://orcid.org/0000-0001-6001-3880
Andrea Nass http://orcid.org/0000-0001-7172-5170
Cathy Quantin-Nataf http://orcid.org/0000-0002-8313-8595
Elliot Sefton-Nash http://orcid.org/0000-0002-5583-4438
Nick Thomas http://orcid.org/0000-0002-0146-0071
Ines Torres http://orcid.org/0000-0003-4180-4905
Jorge L. Vago http://orcid.org/0000-0003-1938-6639
Matthieu Volat http://orcid.org/0000-0002-5184-0304
Francesca Altieri http://orcid.org/0000-0002-6338-8300
Andrea Apuzzo http://orcid.org/0000-0003-2439-6882
Julene Aramendia http://orcid.org/0000-0003-3728-8370
Gorka Arana http://orcid.org/0000-0001-7854-855X
Rickbir Singh Bahia http://orcid.org/0000-0002-6286-7967
Steven G. Banham http://orcid.org/0000-0003-1206-1639
Robert Barnes http://orcid.org/0000-0001-7864-4824
Alexander M. Barrett http://orcid.org/0000-0003-3441-9216
Wolf-Stefan Benedix http://orcid.org/0000-0002-7325-1682
Anshuman Bhardwaj http://orcid.org/0000-0002-2502-6384
Sarah Jane Boazman http://orcid.org/0000-0003-4694-0818
Tomaso R. R. Bontognali http://orcid.org/0000-0003-4917-0388
John Bridges http://orcid.org/0000-0002-9579-5779
Benjamin Bultel http://orcid.org/0000-0002-7084-9574
Valérie Ciarletti http://orcid.org/0000-0001-9483-0539
Maria Cristina De Sanctis http://orcid.org/0000-0002-3463-4437
Zach Dickeson http://orcid.org/0000-0001-9116-2571
Elena A. Favaro http://orcid.org/0000-0001-6126-5465
Marco Ferrari http://orcid.org/0000-0002-7447-6146
Frédéric Foucher http://orcid.org/0000-0002-6037-8633
Walter Goetz http://orcid.org/0000-0001-7998-8995
Albert F. C. Haldemann http://orcid.org/0000-0003-3741-8841
Elise Harrington http://orcid.org/0000-0002-5218-8346
Angeliki Kapatza http://orcid.org/0000-0001-7718-407X
Detlef Koschny http://orcid.org/0000-0001-8690-3507
Agata M. Krzesinska http://orcid.org/0000-0002-0896-3560
Alice Le Gall http://orcid.org/0000-0002-9023-4868
Stephen R. Lewis http://orcid.org/0000-0001-7237-6494
Tanya Lim http://orcid.org/0000-0001-9666-3930
Juan Manuel Madariaga http://orcid.org/0000-0002-1685-6335
Benjamin James Man http://orcid.org/0000-0001-9056-6072
Lucia Mandon http://orcid.org/0000-0002-9310-0742
Nicolas Mangold http://orcid.org/0000-0002-0022-0631
Javier Martin–Torres http://orcid.org/0000-0001-6479-2236
Joseph D. McNeil http://orcid.org/0000-0002-8700-6450
Antonio Molina http://orcid.org/0000-0002-5038-2022
Andoni G. Moral http://orcid.org/0000-0002-6190-8560
Sara Motaghian http://orcid.org/0000-0003-2956-6828
Sergei Nikiforov http://orcid.org/0000-0002-7221-8602
Andrea Pacifici http://orcid.org/0000-0002-2777-2479
Adam Parkes Bowen http://orcid.org/0000-0001-9838-9306
Dirk Plettemeier http://orcid.org/0000-0001-8229-3932
Alfiah Rizky Diana Putri http://orcid.org/0000-0002-2601-6081
Ottaviano Ruesch http://orcid.org/0000-0002-1550-5656
Lydia Sam http://orcid.org/0000-0003-3181-2960
Christian Schröder http://orcid.org/0000-0002-7935-6039
Christoph Statz http://orcid.org/0000-0002-3339-403X
Rebecca Thomas http://orcid.org/0000-0003-1716-9964
Daniela Tirsch http://orcid.org/0000-0001-5905-5426
Zsuzsanna Toth http://orcid.org/0000-0002-6321-5637
Stuart Turner http://orcid.org/0000-0001-9980-3804
Stephanie C. Werner http://orcid.org/0000-0001-5704-0909
Frances Westall http://orcid.org/0000-0002-1938-5823
Barry J. Whiteside http://orcid.org/0000-0001-7877-6886
Rebecca M. E. Williams http://orcid.org/0000-0003-1571-6952
Jack Wright http://orcid.org/0000-0003-0481-0863
Maria-Paz Zorzano http://orcid.org/0000-0002-4492-9650

References

Anderson, R. C., Dohm, J. M., Golombek, M. P., Haldemann, A. F. C., Franklin, B. J., Tanaka, K. L., Lias, J., & Peer, B. (2001). Primary centers and secondary concentrations of tectonic activity through time in the western hemisphere of Mars. *Journal of Geophysical Research: Planets*, *106*(E9), 20563–20585. https://doi.org/10.1029/2000JE001278

Apuzzo, A., Schmidt, G. W., Cianfarra, P., Frigeri, A., & Salvini, F. (2021). Tectonic-related fractures in Oxia Planum (Mars) and their implication for life investigation. In *Proceedings of the 52nd Lunar and Planetary Science Conference* (p. 2082). LPI and the Luna and Planetary Science Institute.

Balme, M. R., Curtis-Rouse, M. C., Banham, S., Barnes, D., Barnes, R., Bauer, A., Bedford, C. C., Bridges, J. C., Butcher, F. E. G., Caballo-Perucha, P., Caldwell, A., Coates, A. J., Cousins, C., Davis, J. M., Dequaire, J., Edwards, P., Fawdon, P., Furuya, K., Gadd, M., … Yeomans, B. (2019). The 2016 UK Space Agency Mars Utah rover field investigation (MURFI). *Planetary and*

Space Science, *165*, 31–56. https://doi.org/10.1016/j.pss.2018.12.003

Barnes, J. W., & Lisle, R. J. (2013). *Basic geological mapping*. John Wiley & Sons.

Barrett, A. M., Balme, M. R., Woods, M., Karachalios, S., Petrocelli, D., Joudrier, L., & Sefton-Nash, E. (2022). NOAH-H, a deep-learning, terrain classification system for Mars: Results for the ExoMars Rover candidate landing sites. *Icarus*, *371*, 114701. https://doi.org/10.1016/j.icarus.2021.114701

Barrett, A. M., Wright, J., Favaro, E., Fawdon, P., Balme, M. R., Woods, M. J., Karachalios, S., Bohacek, E., Sefton-Nash, E., & Joudrier, L. (2023). Oxia Planum, Mars, classified using the NOAH-H deep-learning terrain classification system. *Journal of Maps*, *19*(1), 2112777. https://doi.org/10.1080/17445647.2022.2112777

Berman, D. C., Balme, M. R., Michalski, J. R., Clark, S. C., & Joseph, E. C. S. (2018). High-resolution investigations of Transverse Aeolian Ridges on Mars. *Icarus*, *312*, 247–266. https://doi.org/10.1016/j.icarus.2018.05.003

Bibring, J.-P., Hamm, V., Pilorget, C., Vago, J. L., & the MicrOmega Team. (2017). The MicrOmega investigation onboard ExoMars. *Astrobiology*, *17*(6-7), 621–626. https://doi.org/10.1089/ast.2016.1642

Brossier, J., Altieri, F., De Sanctis, M. C., Frigeri, A., Ferrari, M., De Angelis, S., Apuzzo, A., & Costa, N. (2022). Constraining the spectral behavior of the clay-bearing outcrops in Oxia Planum, the landing site for ExoMars "Rosalind Franklin" rover. *Icarus*, *386*, 115114. https://doi.org/10.1016/j.icarus.2022.115114

Bultel, B., Viennet, J.-C., Poulet, F., Carter, J., & Werner, S. C. (2019). Detection of carbonates in Martian weathering profiles. *Journal of Geophysical Research: Planets*, *124*(4), 989–1007. https://doi.org/10.1029/2018JE005845

Calef, F. J., III, Abarca, H., Soliman, T., Abercrombie, S., & Powell, M. (2017, June 12–15). *Multi-Mission geographic information system for science operations: a test case using MSL data (Vol. 1986, p. 7111)* [Presentation]. Third Planetary Data Workshop and the Planetary Geologic Mappers Annual Meeting.

Calef, F. J., III, & Soliman, T. (2019). *NASA-AMMOS MMGIS open source software*. Retrieved July 14, 2023, from https://github.com/NASA-AMMOS/MMGIS

Carter, J., Loizeau, D., Mangold, N., Poulet, F., & Bibring, J.-P. (2015). Widespread surface weathering on early Mars: A case for a warmer and wetter climate. *Icarus*, *248*(0), 373–382. https://doi.org/10.1016/j.icarus.2014.11.011

Carter, J., Riu, L., Poulet, F., Bibring, J.-P., Langevin, Y., & Gondet, B. (2023). A Mars orbital catalog of aqueous alteration signatures (MOCAAS). *Icarus*, *389*, 115164. https://doi.org/10.1016/j.icarus.2022.115164

Coates, A. J., Jaumann, R., Griffiths, A. D., Leff, C. E., Schmitz, N., Josset, J.-L., Paar, G., Gunn, M., Hauber, E., Cousins, C. R., Cross, R. E., Grindrod, P., Bridges, J. C., Balme, M., Gupta, S., Crawford, I. A., Irwin, P., Stabbins, R., Tirsch, D., … the PanCam Team. (2017). The PanCam instrument for the ExoMars rover. *Astrobiology*, *17*(6-7), 511–541. https://doi.org/10.1089/ast.2016.1548

Cousins, C. R., Gunn, M., Prosser, B. J., Barnes, D. P., Crawford, I. A., Griffiths, A. D., Davis, L. E., & Coates, A. J. (2012). Selecting the geology filter wavelengths for the ExoMars Panoramic Camera instrument. *Planetary and Space Science*, *71*(1), 80–100. https://doi.org/10.1016/j.pss.2012.07.009

Davis, J. M., Balme, M. R., Fawdon, P., Grindrod, P. M., Favaro, E. A., Banham, S. G., & Thomas, N. (2023). Ancient alluvial plains at Oxia Planum, Mars. *Earth and Planetary Science Letters*, *601*, 117904. https://doi.org/10.1016/j.epsl.2022.117904

De Sanctis, M. C., Altieri, F., Ammannito, E., Biondi, D., De Angelis, S., Meini, M., Mondello, G., Novi, S., Paolinetti, R., Soldani, M., Mugnuolo, R., Pirrotta, S., Vago, J. L., & the Ma_MISS team. (2017). Ma_MISS on ExoMars: Mineralogical characterization of the Martian subsurface. *Astrobiology*, *17*(6-7), 612–620. https://doi.org/10.1089/ast.2016.1541

Dickeson, Z. I., & Davis, J. M. (2020). Martian oceans. *Astronomy & Geophysics*, *61*(3), 3.11–3.17. https://doi.org/10.1093/astrogeo/ataa038

DLR. (2019). *HMC-30 regional DTMs and orthoimage Mosaics*. Retrieved July 14, 2023, from https://hrscteam.dlr.de/public/data/regionaldtms.php

Favaro, E. A., Balme, M. R., Davis, J. M., Grindrod, P. M., Fawdon, P., Barrett, A. M., & Lewis, S. R. (2021). The Aeolian environment of the landing site for the ExoMars Rosalind Franklin rover in Oxia Planum, Mars. *Journal of Geophysical Research: Planets*, *126*(4), 2020JE006723. https://doi.org/10.1029/2020JE006723

Favaro, E. A., Balme, M. R., McNeil, J. D., Fawdon, P., Davis, J. M., Grindrod, P. M., & Lewis, S. R. (2024). Periodic bedrock ridges at Oxia Planum and Chryse Planitia, Mars: Evidence for widespread Aeolian erosion of an ancient surface by regional Paleowinds. *Earth and Planetary Science Letters*, *626*, 118522. https://doi.org/10.1016/j.epsl.2023.118522

Fawdon, P., Balme, M., Davis, J., Bridges, J., Gupta, S., & Quantin-Nataf, C. (2022). Rivers and lakes in Western Arabia Terra: The fluvial catchment of the ExoMars 2022 rover landing site. *Journal of Geophysical Research: Planets*, *127*(2), e2021JE007045. https://doi.org/10.1029/2021JE007045

Fawdon, P., Grindrod, P., Orgel, C., Sefton-Nash, E., Adeli, S., Balme, M., Cremonese, G., Davis, J., Frigeri, A., Hauber, E., Le Deit, L., Loizeau, D., Nass, A., Parks-Bowen, A., Quantin-Nataf, C., Thomas, N., Vago, J. L., & Volat, M. (2021). The geography of Oxia Planum. *Journal of Maps*, *17*(2), 621–637. https://doi.org/10.1080/17445647.2021.1982035

Fawdon, P., Orgel, C., Adeli, S., Balme, M., Calef III., F. J., Davis, J. M., Frigeri, A., Grindrod, P., Hauber, E., Le Deit, L., Loizeau, D., Nass, A., Quantin-Nataf, C., Sefton-Nash, E., Thomas, N., Torres, I., Vago, J. L., Volat, M., De Witte, S., … Zorzano, M.-P. (2023). *The high-resolution map of Oxia Planum, Mars; the landing site of the ExoMars Rosalind Franklin rover mission* [Data set]. The Open University ORDO. https://doi.org/10.21954/ou.rd.24147231

Gary-Bicas, C. E., & Rogers, A. D. (2021). Geologic and thermal characterization of Oxia Planum using Mars odyssey THEMIS data. *Journal of Geophysical Research: Planets*, *126*(2), e2020JE006678. https://doi.org/10.1029/2020JE006678

Gunn, M. (2023, November 23). UK Space Agency Enfys anouncment. https://www.gov.uk/government/news/mission-to-explore-life-on-mars-one-step-closer-as-uk-team-to-replace-russian-components-for-mars-rover

Gwinner, K., Jaumann, R., Hauber, E., Hoffmann, H., Heipke, C., Oberst, J., Neukum, G., Ansan, V., Bostelmann, J., Dumke, A., Elgner, S., Erkeling, G., Fueten, F., Hiesinger, H., Hoekzema, N. M., Kersten, E., Loizeau, D., Matz, K.-D., McGuire, P. C., … Willner, K. (2016). The high resolution stereo camera (HRSC) of Mars express and its approach to science analysis and

mapping for Mars and its satellites. *Planetary and Space Science*, *126*, 93–138. https://doi.org/10.1016/j.pss.2016.02.014

Hartmann, W. K., & Neukum, G. (2001). Cratering chronology and the evolution of Mars. *Space Science Reviews*, *96*(1/4), 165–194. https://doi.org/10.1023/A:1011945222010

Ivanov, M. A., Slyuta, E. N., Grishakina, E. A., & Dmitrovskii, A. A. (2020). Geomorphological analysis of ExoMars candidate landing site Oxia Planum. *Solar System Research*, *54*(1), 1–14. https://doi.org/10.1134/S0038094620010050

Kirk, R., Howington-Kraus, E., Rosiek, M. R., Anderson, J. A., Archinal, B. A., Becker, K. J., Cook, D. A., Galuszka, D. M., Geissler, P. E., Hare, T. M., Holmberg, I. M., Keszthelyi, L. P., Redding, B. L., Delamere, W. A., Gallagher, D., Chapel, J. D., Eliason, E. M., King, R., & McEwen, A. S. (2008). Ultrahigh resolution topographic mapping of Mars with MRO HiRISE stereo images: Meter-scale slopes of candidate Phoenix landing sites. *Journal of Geophysical Research: Planets*, *113*(E3), E00A–E024. https://doi.org/10.1029/2007JE003000

Kronyak, R. E., Kah, L. C., Edgett, K. S., VanBommel, S. J., Thompson, L. M., Wiens, R. C., Sun, V. Z., & Nachon, M. (2019). Mineral-filled fractures as indicators of multigenerational fluid flow in the Pahrump hills member of the Murray formation, gale crater, Mars. *Earth and Space Science*, *6*(2), 238–265. https://doi.org/10.1029/2018EA000482

Malin, M. (2007). *MRO context camera experiment data record level 0 V1.0, MRO-M-CTX-2-EDR-L0-V1.0* [Data set]. NASA Planetary Data System. https://doi.org/10.17189/1520266.

Mandon, L., Parkes Bowen, A., Quantin-Nataf, C., Bridges, J. C., Carter, J., Pan, L., Beck, P., Dehouck, E., Volat, M., Thomas, N., Cremonese, G., Tornabene, L. L., & Thollot, P. (2021). Morphological and spectral diversity of the clay-bearing unit at the ExoMars landing site Oxia Planum. *Astrobiology*, *21*(4), 464–480. https://doi.org/10.1089/ast.2020.2292

Mastropietro, M. (2019). *Analysis of Oxia Planum region (Mars): The landing site of the ESA ExoMars 2020 rover*.

McEwen, A. S., Eliason, E. M., Bergstrom, J. W., Bridges, N. T., Hansen, C. J., Delamere, W. A., Grant, J. A., Gulick, V. C., Herkenhoff, K. E., Keszthelyi, L., Kirk, R. L., Mellon, M. T., Squyres, S. W., Thomas, N., & Weitz, C. M. (2007). Mars reconnaissance orbiter's high resolution imaging science experiment (HiRISE). *Journal of Geophysical Research: Planets*, *112*(E5), E05S02. https://doi.org/10.1029/2005JE002605

McNeil, J. D., Fawdon, P., Balme, M. R., & Coe, A. L. (2021). Morphology, morphometry and distribution of isolated landforms in southern Chryse Planitia, Mars. *Journal of Geophysical Research: Planets*, *126*(5), e2020JE006775. https://doi.org/10.1029/2020JE006775

McNeil, J. D., Fawdon, P., Balme, M. R., Coe, A. L., & Thomas, N. (2022). Mounds in Oxia Planum: The burial and exhumation of the ExoMars rover landing site. *Journal of Geophysical Research: Planets*, *127*(11), e2022JE007246. https://doi.org/10.1029/2022JE007246

Michalski, J. R., & Bleacher, J. E. (2013). Supervolcanoes within an ancient volcanic province in Arabia Terra, Mars. *Nature*, *502*(7469), 47–52. https://doi.org/10.1038/nature12482

Molina, A., López, I., Prieto-Ballesteros, O., Fernández-Remolar, D., de Pablo, M. Á., & Gómez, F. (2017). Coogoon Valles, western Arabia Terra: Hydrological evolution of a complex Martian channel system. *Icarus*, *293*, 27–44. https://doi.org/10.1016/j.icarus.2017.04.002

Neukum, G., Jaumann, R., & HRSC Co-Investigator and Experiment Team. (2004). HRSC: The high resolution stereo camera on Mars express. In A. Wilson (Ed.), *Mars express: The scientific payload* (Vols. 1–1240, pp. 17–35). ESA. https://elib.dlr.de/11065/.

Neumann, G. A., Zuber, M. T., & Smith, D. E. (2003). *Mola mission experiment gridded data record* [Data set]. NASA Planetary Data System. https://doi.org/10.17189/1519460.

Noe Dobrea, E. Z., Bishop, J. L., McKeown, N. K., Fu, R., Rossi, C. M., Michalski, J. R., Heinlein, C., Hanus, V., Poulet, F., Mustard, R. J. F., Murchie, S., McEwen, A. S., Swayze, G., Bibring, J.-P., Malaret, E., & Hash, C. (2010). Mineralogy and stratigraphy of phyllosilicate–bearing and dark mantling units in the greater Mawrth Vallis/west Arabia Terra area: Constraints on geological origin. *Journal of Geophysical Research: Planets*, *115*, E00D19. https://doi.org/10.1029/2009JE003351

Pan, L., Quantin-Nataf, C., Breton, S., & Michaut, C. (2019). The impact origin and evolution of Chryse Planitia on Mars revealed by buried craters. *Nature Communications*, *10*(1), 4257. https://doi.org/10.1038/s41467-019-12162-0

Parkes-Bowen, A., Bridges, J., Tornabene, L., Mandon, L., Quantin-Nataf, C., Patel, M. R., Thomas, N., Cremonese, G., Munaretto, G., Pommerol, A., & Pajola, M. (2022). A CaSSIS and HiRISE map of the Clay-bearing Unit at the ExoMars 2022 landing site in Oxia Planum. *Planetary and Space Science*, *214*, 105429. https://doi.org/10.1016/j.pss.2022.105429

Quantin-Nataf, C., Carter, J., Mandon, L., Thollot, P., Balme, M., Volat, M., Pan, L., Loizeau, D., Millot, C., Breton, S., Dehouck, E., Fawdon, P., Gupta, S., Davis, J., Grindrod, P. M., Pacifici, A., Bultel, B., Allemand, P., Ody, A., … Broyer, J. (2021). Oxia Planum: The landing site for the ExoMars "Rosalind Franklin" rover mission: Geological context and prelanding interpretation. *Astrobiology*, *21*(3), 345–366. https://doi.org/10.1089/ast.2019.2191

Quantin-Nataf, C., Lozac'h, L., Thollot, P., Loizeau, D., Bultel, B., Fernando, J., Allemand, P., Dubuffet, F., Poulet, F., Ody, A., Clenet, H., Leyrat, C., & Harrisson, S. (2018). MarsSI: Martian surface data processing information system. *Planetary and Space Science*, *150*, 157–170. https://doi.org/10.1016/j.pss.2017.09.014

Riu, L., Carter, J., Poulet, F., Cardesín-Moinelo, A., & Martin, P. (2023). Global surficial water content stored in hydrated silicates at Mars from OMEGA/MEx. *Icarus*, *398*, 115537. https://doi.org/10.1016/j.icarus.2023.115537

Roberts, A. L., Fawdon, P., & Mirino, M. (2021). Impact crater degradation, Oxia Planum, Mars. *Journal of Maps*, *17*(2), 581–590. https://doi.org/10.1080/17445647.2021.1976685

Sefton-Nash, E., Balme, M. R., Quantan-Nataf, C., Fawdon, P., Volat, M., Hauber, E., Orgel, C., Ruesch, O., Frigeri, A., & Vago, J. L. (2020). HiRISE scale charectorization of the Oxia Planum landing site for the ExoMars Rosalind Frankin Rover. *Preceedings of the 51st Luna and Planetary Science Conference*, #2417. https://www.hou.usra.edu/meetings/lpsc2020/pdf/2417.pdf

Silvestro, S., Pacifici, A., Salese, F., Vaz, D. A., Neesemann, A., Tirsch, D., Popa, C. I., Pajola, M., Franzese, G., Mongelluzzo, G., Ruggeri, A. C., Cozzolino, F., Porto, C., & Esposito, F. (2021). Periodic bedrock ridges at the

ExoMars 2022 landing site: Evidence for a changing wind regime. *Geophysical Research Letters*, *48*(4), e2020GL091651. https://doi.org/10.1029/2020GL091651

Skinner, J. A., Huff, A. E., Black, S. R., Buban, H. C., Fortezzo, C. M., Gaither, T. A., Hare, T. M., & Hunter, M. A. (2022). *Planetary Geologic Mapping protocol—2022* (Report No. 11-B13) (p. 28). https://doi.org/10.3133/tm11B13.

Smith, D. E., Zuber, M. T., Frey, H. V., Garvin, J. B., Head, J. W., Muhleman, D. O., Pettengill, G. H., Phillips, R. J., Solomon, S. C., Zwally, H. J., Banerdt, W. B., Duxbury, T. C., Golombek, M. P., Lemoine, F. G., Neumann, G. A., Rowlands, D. D., Aharonson, O., Ford, P. G., Ivanov, A. B., … Sun, X. (2001). Mars Orbiter Laser Altimeter: Experiment summary after the first year of global mapping of Mars. *Journal of Geophysical Research: Planets*, *106*(E10), 23689–23722. https://doi.org/10.1029/2000JE001364

Stack, K. M., Williams, N. R., Calef, F., Sun, V. Z., Williford, K. H., Farley, K. A., Eide, S., Flannery, D., Hughes, C., Jacob, S. R., Kah, L. C., Meyen, F., Molina, A., Nataf, C. Q., Rice, M., Russell, P., Scheller, E., Seeger, C. H., Abbey, W. J., … Aileen Yingst, R. (2020). Photogeologic map of the perseverance rover field site in Jezero Crater constructed by the Mars 2020 science team. *Space Science Reviews*, *216*(8), 127. https://doi.org/10.1007/s11214-020-00739-x

Sun, V. Z., & Stack, K. M. (2020). *Geologic map of Jezero crater and the Nili Planum region, Mars* (Report No. 3464) (p. 14). https://doi.org/10.3133/sim3464.

Tanaka, K. L., Skinner, J. A., Dohm, J. M., Irwin, R. P., III, Kolb, E. J., Fortezzo, C. M., Platz, T., Michael, G. G., & Hare, T. M. (2014). Geologic map of Mars: U.S. Geological Survey Scientific Investigations Map 3292, Scale 1:20,000,000, pamphlet 43 p. http://pubs.usgs.gov/sim/3292/.

The Murry Lab. (2023). *The Global CTX Mosaic of Mars*. https://murray-lab.caltech.edu/CTX/

Thomas, N., Cremonese, G., Ziethe, R., Gerber, M., Brändli, M., Bruno, G., Erismann, M., Gambicorti, L., Gerber, T., Ghose, K., Gruber, M., Gubler, P., Mischler, H., Jost, J., Piazza, D., Pommerol, A., Rieder, M., Roloff, V., Servonet, A., … Wray, J. J. (2017). The colour and stereo surface imaging system (CaSSIS) for the ExoMars trace Gas orbiter. *Space Science Reviews*, *212*(3), 1897–1944. https://doi.org/10.1007/s11214-017-0421-1

Tornabene, L. L., Seelos, F. P., Pommerol, A., Thomas, N., Caudill, C. M., Becerra, P., Bridges, J. C., Byrne, S., Cardinale, M., Chojnacki, M., Conway, S. J., Cremonese, G., Dundas, C. M., El-Maarry, M. R., Fernando, J., Hansen, C. J., Hansen, K., Harrison, T. N., Henson, R., … Wray, J. J. (2017). Image simulation and assessment of the colour and spatial capabilities of the colour and stereo surface imaging system (CaSSIS) on the ExoMars trace gas orbiter. *Space Science Reviews*, *214*(1), 18. https://doi.org/10.1007/s11214-017-0436-7

Uthus, T. N. (2020). *Crater statistics and Geological history of Oxia Planum, landing site for ExoMars2022*.

Vago, J. L., Spoto, F., & Bauer, M. (2018, September 11). *Oxia Planum favoured for ExoMars surface mission*. https://exploration.esa.int/web/mars/-/60914-oxia-planum-favoured-for-exomars-surface-mission.

Vago, J. L., Westall, F., Pasteur Instrument Teams, Landing, S., Coates, A. J., Jaumann, R., Korablev, O., Ciarletti, V., Mitrofanov, I., Josset, J.-L., De Sanctis, M. C., Bibring, J.-P., Rull, F., Goesmann, F., Steininger, H., Goetz, W., Brinckerhoff, W., Szopa, C., Raulin, F., … Carreau, C. (2017). Habitability on Early Mars and the Search for Biosignatures with the ExoMars Rover. *Astrobiology*, *17*(6-7), 471–510. https://doi.org/10.1089/ast.2016.1533

Volat, M., & Quantan-Nataf, C. (2020). *Oxia HiRISE DEM mosaic*. https://doi.org/10.48326/idoc.psup.marssi.hirise.oxia.

Volat, M., Quantin-Nataf, C., & Dehecq, A. (2022). Digital elevation model workflow improvements for the MarsSI platform and resulting orthorectified mosaic of Oxia Planum, the landing site of the ExoMars 2022 rover. *Planetary and Space Science*, *222*, 105552. https://doi.org/10.1016/j.pss.2022.105552

Warner, N. H., Gupta, S., Calef, F., Grindrod, P., Boll, N., & Goddard, K. (2015). Minimum effective area for high resolution crater counting of Martian terrains. *Icarus*, *245*, 198–240. https://doi.org/10.1016/j.icarus.2014.09.024

Woodley, S. Z., Fawdon, P., Balme, M. R., & Rothery, D. A. (2023). Map of tectonic shortening structures in Chryse Planitia and Arabia Terra, Mars. *Journal of Maps*, *19*(1), 2251514. https://doi.org/10.1080/17445647.2023.2251514